



Kent Academic Repository

D'Arcy, Emma (2020) *A Study of Light-curves of Nearby Dipper YSOs to Determine Circumstellar Disk Properties*. Master of Science by Research (MScRes) thesis, University of Kent,.

Downloaded from

<https://kar.kent.ac.uk/82130/> The University of Kent's Academic Repository KAR

The version of record is available from

This document version

UNSPECIFIED

DOI for this version

Licence for this version

UNSPECIFIED

Additional information

Versions of research works

Versions of Record

If this version is the version of record, it is the same as the published version available on the publisher's web site. Cite as the published version.

Author Accepted Manuscripts

If this document is identified as the Author Accepted Manuscript it is the version after peer review but before type setting, copy editing or publisher branding. Cite as Surname, Initial. (Year) 'Title of article'. To be published in *Title of Journal*, Volume and issue numbers [peer-reviewed accepted version]. Available at: DOI or URL (Accessed: date).

Enquiries

If you have questions about this document contact ResearchSupport@kent.ac.uk. Please include the URL of the record in KAR. If you believe that your, or a third party's rights have been compromised through this document please see our [Take Down policy](https://www.kent.ac.uk/guides/kar-the-kent-academic-repository#policies) (available from <https://www.kent.ac.uk/guides/kar-the-kent-academic-repository#policies>).

A Study of Light-curves of Nearby Dipper YSOs to Determine Circumstellar Disk Properties

Author:

Emma D'Arcy

Supervisor:

Dr. Dirk Froebrich

A thesis presented for the degree of Master of Science (MSc)



Centre of Astrophysics and Planetary Science
School of Physical Sciences
University of Kent

July 7, 2020

Abstract

The magnitudes of nearby young stellar objects, recorded in three filters (visual, red, and infra-red), have been observed by the Beacon Observatory since September 2015. Using the data up until November 2017, the light-curves of the objects were studied for the presence of dipper stars. The long term changes in magnitude were taken into account when searching for short dips caused by increased density of material along the line of sight in the inner disk. The depth and duration of these dips were observed and used alongside basic assumptions of stellar mass and distance from the star to estimate the mass and dimensions of material clumps in the inner disk.

This was done so as to better understand the evolution of young stars, and the structure of accretion disks. The parameters of the dips found were consistent with previous work on the topic, and provide the starting blocks to produce a structural model of the inner disks of young stars.

Declaration

I declare that this thesis, titled "A study of light-curves of nearby dipper YSOs to determine circumstellar disk properties" is the result of my own research, and has not been previously submitted for assessment. Where the work of others has been consulted, and any contribution from other parties has been included, it is explicitly stated in the text.

Signed:

Date:

Acknowledgements

I would firstly like to thank my supervisor Dr Dirk Froebrich for giving me the opportunity to perform this research, and for his guidance throughout the project. I would also like to thank Dr Timothy Kinnear for his assistance and teachings that helped make the code functional.

I also wish to thank my parents, Brian and Julia D'Arcy for their unconditional love and support throughout everything I do. Finally I thank all my family and friends for all of their support and encouragement.

Contents

List of Figures	5
1 Background - Young Stellar Objects	8
1.1 Young Stellar Objects	8
1.1.1 Pre Main Sequence Stars	8
1.1.2 Dipper Stars	10
1.2 Circumstellar Disks	10
1.3 Planet Formation	11
2 Background - Light-Curves and Disk Structure	12
2.1 Light-Curves	12
2.2 Magnitude	13
2.2.1 Stellar Variability	13
2.2.2 magnitude dips as a result of occultations	14
3 Method	16
3.1 Targets and observation	16
3.1.1 Observed Targets	16
3.1.2 Beacon Observatory and Observations	18
3.2 Defining a Dip	22
3.3 Measuring Dip Properties	23
3.4 Calculating Radius and Mass	27
3.5 Material density and dust growth	28

4	Results	31
4.1	Identifying Dips	31
4.1.1	Single Data Point Dips	31
4.1.2	Effect of filter width of dip detection	33
4.2	Dip Depth	41
4.3	Duration	41
4.4	Material Dimensions	43
4.5	Mass	50
4.6	Grain size	54
5	Conclusions	57

List of Figures

3.1	<i>Histogram of distribution of cadence between observation for target NGC7129 . . .</i>	19
3.2	<i>Histogram of distribution of cadence between observation for target IC5070 . . .</i>	20
3.3	<i>Histogram of distribution of cadence between observation for target IC1396A . . .</i>	21
3.4	<i>Diagram of an example lightcurve showing the dip parameters measured. These are: maximum duration; time difference in days between two data points either side of a dip, minimum duration; time difference in days between the first and last points in a dip, and dip depth; the magnitude difference between the median magnitude, and the average magnitude of the points in a dip</i>	24
3.5	<i>Histogram of the distribution of both the minimum and maximum durations for all analysed. The minimum duration is shown in blue, and the maximum duration in green.</i>	26
3.6	<i>An example v against V-I plot</i>	30
4.1	<i>Light-curve for object J21371591 in cluster IC1396A. The top curve shows the magnitude of the star in the 3 filters used to record data, green represents the visual filter, red represents the red filter, and blue shows the infra-red filter. The middle plot shows the flattened light-curve in the visual filter, with data points in dips highlighted in red. The final plot shows the original light-curve with dips also highlighted in red.</i>	34
4.2	<i>Light-curve for the object GM Cep, in the cluster IC1396A. The top, middle, and bottom plots showing the full light-curve in all 3 filters that magnitude was recorded in, the filtered light-curve in the visual filter, and the original light-curve in the visual filter respectively</i>	35

4.3	<i>Light-curve for the object GM Cep in the cluster IC1396A with a smoothing filter of 250 days. The top, middle, and bottom plots showing the full light-curve in all 3 filters that magnitude was recorded in, the flattened light-curve in the visual filter, and the original light-curve in the visual filter respectively. All dips are highlighted in red.</i>	36
4.4	<i>Light-curve for GM Cep from April 2016 to present (September 2018). The data from the visual filter is displayed in green, and the infra-red data displayed in black.</i>	38
4.5	<i>Light-curves for object J03444011 in cluster IC148</i>	39
4.6	<i>Light-curves of object J03444011 in cluster IC148 with a 50 day filter width</i>	40
4.7	<i>Histogram of the distribution of the dip depth for every dip analysed with a logarithmic y axis</i>	44
4.8	<i>Histogram of the distribution of the average duration for every dip analysed with a logarithmic y axis</i>	45
4.9	<i>Histogram of the distribution of average dip duration for all analysed dips shorter than 30 days</i>	46
4.10	<i>Histogram of the distribution of the estimate dimensions of material calculated for every dip analysed</i>	47
4.11	<i>Histogram of the distribution of dimensions less than 0.75AU.</i>	48
4.12	<i>histogram of distribution of the estimate mass of material occulting the star, calculated for every dip analysed, displayed in lunar masses</i>	51
4.13	<i>Histogram of the distribution of mass values below 0.1 Lunar Masses</i>	52
4.14	<i>Histogram of the density distribution across all dips analysed.</i>	53
4.15	<i>Figure of the distribution of the values of the slopes of the V against V-I plots, in degrees.</i>	56

Chapter 1

Background - Young Stellar Objects

1.1 Young Stellar Objects

1.1.1 Pre Main Sequence Stars

The term Young Stellar Objects (YSOs) covers stars at any stage from their initial formation (protostars) until they reach the Main sequence (MS) stage. Most lower mass stars will take around 10 Myr to reach the MS stage of their existence, although this value relies heavily on the mass of the star. Class 0 are the youngest protostars, with a mass lower than that of the star's surrounding gas and dust envelope, from which it accretes material. A protostar is considered a class I star when its mass exceeds that of the gas and dust envelope (Andre, Ward-Thompson, and Barsony, 2000). As low mass stars gain material and the envelope of material surrounding them shifts into a disk, they are classed as T-Tauri stars. T-Tauri stars are young, low mass objects with flattened circumstellar disks of material left over from the star's initial collapse (Adams, Lada, and Shu, 1987, Johnstone et al., 2014). The circumstellar disk surrounding T Tauri stars allows for accretion of material until the star reaches MS, and is the birthplace of planetary systems. This means the observation of T Tauri stars can provide insight into the evolution of young

stars and the structure of circumstellar disks, this will be discussed more in section 1.2.

There are 2 types of T Tauri stars; classical T Tauri stars (CTTS), and weak-line T Tauri stars (WTTS). These are also known as class II and class III stars respectively, with class II (CTTS) being the younger of the two classes (Adams, Lada, and Shu, 1987). CTTS are recognisable by their strong $H\alpha$ emission line, characteristic of accretion of material from the disk to the star. The inner disk surrounding a CTTS is optically thick, rich in gas and sub-mm particles. The material in the inner disk, absorbs UV output from the star and re-emits it as near infra-red radiation (Meng et al., 2017). This results in giving the star a spectral emission with a strong infra-red excess. At this stage, the average accretion rate of the star will still be quite high, with some dust growth occurring in areas of the disk further from the star.

Class III (WTTS) are generally described as the evolutionary successors to class II stars. It has been well accepted that WTTS have optically thin disks due to much of the material from the inner disk having already been accreted to the star. As such, the star is left with a depleted inner disk, lacking in gas and dust. While the inner disk is depleted, larger particles are present further out in the disk, which in time will evolve in to planets. The depleted inner disk results in a lower accretion rate, giving the star a weak $H\alpha$ line, and the classification of WTTS (McCabe, 2004). However, there have been recent observations of WTTS with gaps in their disks, or where their disks have separated into rings (Engler et al., 2019). These features are thought to be related to planet formation, and provide a more efficient environment for planet growth (Bae, Zhu, and Hartmann, 2017).

The observation of young, high mass ($>3 M_{\odot}$) stars is complex due to the effects a high mass star has on its surroundings. Higher mass protostars are at first surrounded by a thick gas and dust envelope, which makes visual observations difficult (Yorke and Kruegel, 1977). A massive star's high luminosity and strong stellar winds disturbs its surrounding material, causing it to behave differently to the disks around lower mass stars (Gruendl and Chu, 2009). This thesis focuses on the analysis of lower mass YSOs.

1.1.2 Dipper Stars

Dipper stars are young stars that experience short (hours to days), severe dips in magnitude. As the dips are caused by warps and clumps of material in a stars' inner disk, dippers are generally CTTS (Cody et al., 2014). They can be spotted by searching for variable stars with a strong near infra-red excess spectrum. The effect that clumps of material have on a star's output can be deduced by observing how the infra-red excess changes during dips (Hedges, Hodgkin, and Kennedy, 2018). Such dipper stars are the primary targets for this thesis, which intends to use the parameters of magnitude dips to build a better understanding of disk structure. The intention is to estimate the physical properties of clumps of dust in circumstellar disks by measuring the parameters of dips in YSOs' light-curves. To do so with a large sample of YSOs of varying ages will provide basic information on the structure of the inner disk region. It is hoped this will help to better the understanding of circumstellar disks and the activity of stellar material, including planet formation.

1.2 Circumstellar Disks

When the core of a gas and dust cloud collapses to form a protostar, the remaining material is left as an envelope around the new star. Over time, this material shifts into a flattened disk around the stars rotational axis, as a way of conserving angular momentum (Dunham et al., 2014). The material is forced into rotating channels that spiral towards the star, following magnetic field lines. Material closer to the star has a higher temperature and radial velocity than the more distant material (Gillen et al., 2017).

Much of the material in the inner disk will be accreted on to the star. Initially, a protostar will rely on accretion to provide outward pressure to counteract the star's self gravity and prevent collapse, thus maintaining its shape (Adams, Lada, and Shu, 1987), and although accretion continues as the star becomes more stable, there is a steady decrease in accretion rate as the star develops and the disk becomes depleted. Other factors such as

fluctuations in density of material in the disk cause changes in accretion rate. There are also cases of extreme changes in accretion rate (discussed in section 2.2.1), although these are not well understood.

A circumstellar disk can be observed through a star's spectral emission. As mentioned previously, the shape of a star's spectral energy distribution is indicative of its accretion rate. In younger stars with material dense disks, the hot, small particles of the inner disk re-emit some of the star's output into near infra-red radiation. Cooler, larger, particles further from the YSO re-emit far infra-red radiation. As this material is still present after the inner disk becomes depleted, far infra-red emission can be used to characterise a protoplanetary disk.

All material within a circumstellar disk is entirely used up or lost by the time the star reaches main sequence, normally taking between 1-10 Myr (Herbst, 2012). As well as through accretion, material is lost from the disk via material outflows at the star's rotational poles that form to conserve angular momentum. Smaller particles escape the disk through photoevaporation, particularly as the accretion rate slows. Other particles in a disk are likely to be used in planet formation (Bitsch et al., 2015).

1.3 Planet Formation

The process of planet formation takes millions of years. The formation of terrestrial planets begins with grain growth in the circumstellar disk. Small particles in the disk collide and stick together (Bitsch et al., 2015). This reduces the speed of particles, and dust density increases in the mid-plane of the disk. The larger particles formed from smaller particles have a stronger gravitational pull, which attracts smaller particles and so dust growth continues (Williams and Cieza, 2011). Eventually, the material evolves into large rocks and boulders which continue to interact in more violent collisions until a stable planetary system is in existence around the central star. There is evidence to suggest that dust growth starts early in a star's lifetime, while the disk is still rich in gas. A gas rich disk also has ideal conditions for the formation of gas giant planets (Bitsch et al., 2015).

Chapter 2

Background - Light-Curves and Disk Structure

2.1 Light-Curves

Light-curves are a display of how an object's magnitude changes over time. Observing and plotting the magnitude of a star in multiple different filters allows the colour and temperature of a star to be calculated. By giving a compact, visual display of how magnitude fluctuates in different filters, they can be used to gather information on the cause of magnitude fluctuations of stars. For example, a strong drop in all filters indicates the presence of optically thick material around the star, or a greater drop in the red filter than the visual filter could be due to an increase in accretion rate (Guo et al., 2018). Cold spots on the star's surface and disk warps also cause changes in the colour and flux of a star. By taking the depth and duration of dips from occultations by material in the disk, the dimensions of clumps of material in the disk can be calculated. With enough data, such information can be used to estimate the structure of a young star's inner disk. Due to the variability of young stars, measures were taken to ensure only dips due to occultations were analysed, these will be discussed in section 3.2. Similar work has been

done with a smaller data sample than the one used in this thesis by (Hedges, Hodgkin, and Kennedy, 2018), where a series of algorithms were used to find dipper stars amongst young variable stars. The parameters of the dips were recorded and the distribution of dip depth and duration was observed.

2.2 Magnitude

2.2.1 Stellar Variability

As well as their spectral emission, T Tauri stars are defined by their low luminosity and irregular variability (Joy, 1945). There are multiple causes of variation in magnitude of YSOs and they act over different time frames and have different effects on magnitude. This complicates singling out occultations from material and warps in an accretion disk. Smoothing the light-curve of an object with a suitable width filter (see section 3.2) makes finding the desired dips more probable. When analysing a large sample, an understanding of the time frame of different causes of variability allows a general filter width to be estimated. Any objects where the chosen filter width is not suitable can be picked out by eye and treated individually.

Particularly in the earliest stages of a star's development, its magnitude is at least in part dependent on its accretion. Initially the accretion rate of a star will be quite high as the star becomes more stable. Over millions of years, the average accretion rate will slow as the disk depletes of gas and sub mm particles. As material is funnelled on to a star, accretion is focused onto points on a star, increasing the temperature at these spots on a star's surface (Johns-Krull, Valenti, and Koresko, 1999). The increased temperature means these hot spots are brighter than the rest of the star, these hot spots are visible as the star rotates, causing frequent fluctuations in magnitude with the severity dependent on accretion rate. Accretion has a strong impact on a star's magnitude, in cases of episodic accretion, a large increase in the accretion rate leads to a burst in magnitude (Audard et al., 2014). After the burst in magnitude, the accretion will revert back to its average

rate over a time frame of months to years. There is little understanding of the exact causes of these sudden increases in accretion rate, and their stochastic nature makes their causes hard to predict. However they are speculated to be caused by changes in density in the accretion disk, or from material falling from the protostellar envelope, towards the disk (Audard et al., 2014). These changes are seen particularly in CTTS, where the inner disk is still rich in gas and dust and there is a strong accretion emission line (M.Fernandez, 1996).

There is a direct link between the temperature of a star and its magnitude, while hot spots on a stellar surface show an increase in flux, cool spots show up as a dip in flux. Cool spots will produce periodic dips in a light-curve every time they are in line of sight as a star rotates (Herbst, 2012). Due to the typical rotation period of YSOs these dips will show up frequently; more so in WTTS, which have a tendency to rotate faster than CTTS (Bouvier et al., 1993). Their frequency and duration would suggest that cool spots are most likely to be mistaken for dips from occultations of material in the inner disk. However, should an object have very few hot or cool spots, their behaviour will appear sinusoidal, and so will be removed while smoothing the curve, if there are many hot and cool spots, there will be no fixed pattern, the star's magnitude will vary frequently and smaller dips risk becoming lost in filtering the curve. Occultations from the circumstellar disk appear in a more irregular pattern as the material in the disk shifts over time. As well as this, the material will be at varying distances from the star, and orbiting at different speeds, resulting in apparently stochastic dips in magnitude.

2.2.2 magnitude dips as a result of occultations

As well the long term fluctuation in magnitude, TTS also experience short term (hours to days) severe (10% -50% of the star's magnitude (Hedges, Hodgkin, and Kennedy, 2018) dips in magnitude. These stars are known as dipper stars. Such dips are the result of clumps of material of increased density within the circumstellar disk blocking the optical output of the star. For CTTS, these dips are likely caused by clumps and warps in the stars inner disk. For older, WTTS, these dips will be caused by the remaining material in their

outer disk, analysis of these dips would show the structure of the star’s protoplanetary disk.

In order for a dip to occur as a result of occultation of material, a clump of material of increased density compared to the rest of the disk must pass in front of the star along our line of sight. Due to the flattened nature of circumstellar disks, it is reasonable to assume that not all YSOs with disks would show occultation dips. If a disk is not edge-on to our line of sight then its material would not block a YSOs emission, and an occultation dip would not be noticeable (Williams and Cieza, 2011). However, a completely edge on disk at 90° would cause too large an amount of material along the line of sight for the star to be distinguishable as a YSO, particularly for gas and dust rich CTTS. As such it has been calculated that the best angle for observing an accretion disk is between 65° and 70° (Chiang and Goldreich, 1999). Despite this, there is evidence to suggest that there are exceptions to this requirement. A small study by Ansdell et al., 2016a, shows YSOs with near face on disks still showing dipper star behaviour. The study comes with the suggestion of rethinking the specific requirements for dipper stars and observations of the inner disk.

The method by which occultation dips are defined will be covered in section 3.2. Once defined, the colour change of the star during a dip will be observed to determine the nature of the material in the disk. When material in the inner disk causes a magnitude dip in the visual filter, it due a clump of material with a higher column density than the rest of the disk. As a result there is more material present along the line of sight to re-emit the star’s output as near infra-red radiation (Guarcello et al., 2017). The expected infra-red excess can be observed through calculating the total to selective extinction ratio R_v . For most dipping young stars this value is often around 3.1.

Chapter 3

Method

3.1 Targets and observation

3.1.1 Observed Targets

For this project, the data from eight nearby (< 1 kpc) targets, all less than 5 Myr, old were used (IC1396A, IC348, IC5146, IC5070, NGC1333, NGC2244, NGC2264, NGC7129). These targets were chosen for their significant collection of dipping YSOs.

IC1396A is a dark globule often referred to as the Elephant Trunk nebula. It is believed to be a highly active star forming region. The globule is located in the IC 1396 H_{II} region in the Cepheus constellation (Getman et al., 2012). The globule is estimated to be 750pc from Earth, and to be around 27pc in diameter (Reach et al., 2004, Matthews, 1979). It also has a high density of class II T Tauri stars with more developed circumstellar disks (Schmeja, Klessen, and Froebrich, 2005).

Also in the Cepheus region, roughly 1kpc from Earth and with a radius of 0.9pc, is the NGC7129 cluster (Megeath et al., 2004). It is around 3Myr old (Straizys et al., 2014) with a high population of young stars, including class II and III stars. Many stars in the cluster are at an age when accretion disks often disappear (Stelzer and Scholz, 2009), making

them suitable for the observation of planet formation.

The young cluster IC348 is found in the Perseus molecular cloud (Lada and Lada, 1995). The cluster is thought to be around 2Myr old, around 315pc from Earth and have a diameter of 20pc. it is densely populated, with over 400 members (Luhman et al., 2003). Most of the objects are young stars such as classical T Tauri stars, there is also a large population of young brown dwarfs. The work of Haisch, Lada, and Lada, 2001; found that $65 \pm 8\%$ of YSOs in the cluster showed infra-red excess and evidence of an inner circumstellar disk. The Perseus molecular cloud also contains the nebula NGC1333. NGC1333 is an active star forming region at a distance of around 350pc from Earth, containing a high number of young T Tauri stars (Strom, Grasdalen, and Strom, 1974, Ungerechts and Thaddeus, 1987).

IC5146 is a young cluster situated within the Cygnus constellation that, like other target, contains YSOs which make it suitable for observation (Lada et al., 1994). The cluster lies at a distance of around 900pc to 1kpc from Earth, slightly to the east of a dark cloud complex which has been the subject of multiple previous studies (Elias, 1978, Harvey et al., 2008).

The Pelican Nebula (IC5070) lies close to the North American Nebula (NGC700) and is a H_{II} star forming region (Bally and Scoville, 1980). As with all targets for this project, it had a high number of YSOs, many of which are variable T Tauri stars (Ibryamov et al., 2018). IC 5070 is a well observed nebula, which has led to the observations of several objects of interest, including potentially quasi-periodic stars. These are interesting for their ability to allow the calculation of material distance from the central star (Froeblich et al., 2018b)

Both NGC2244 and NGC 2264 lie in the Monoceros constellation. With NGC2244 in the Rosette nebula (Park and Sung, 2002) at 1600pc, and NGC2264 around 800pc away (Cody et al., 2014), though there is some uncertainty in the distance of both targets (Perez, The, and Westerlund, 1987). NGC2264 is a roughly 5Myr old cluster with the median age of a resident star being around 1.1Myr. Dahm and Simon, 2005; states that of the YSOs observed in 2264, 241 were T Tauri stars displaying periodic variability, along with

123 irregular variable stars. The NGC2244 cluster is considered to be between 1.7-2.5Myr old and is also a star forming region containing young variable stars as well as a binary system (Hensberge, Pavlovski, and Verschueren, 2000).

3.1.2 Beacon Observatory and Observations

The data used for this project comes from the HOYS-CAPS (Hunting Outbursting Young Stars with the Centre of Astrophysics and Planetary Science) project. Most of this data comes from the Beacon observatory. The Beacon observatory is located at the University of Kent at 51.296633° North, 1.053267° East. It contains a 17" PlaneWave CDK telescope with a 4K by 4K CCD and Peltier cooler. The filter wheel contains 5 filters; B, V, R, I, and H α . For this project, data from just the V, R, and I filters was used. The camera has a field of view of 1° X 1° although the corners of the images are highly vignetted, leaving a useful field of view equivalent to a circle of 1° diameter (Froebrich et al., 2018a). A small portion of the data comes from a community of amateur astronomers with their own telescopes.

Before observations start for a night, a series of dark frames are taken with the telescope shutters closed. These frames are later subtracted from images to cancel out any hot pixels on the CCD. Flat field frames are also taken, which are a series of twelve one second frames taken shortly after sunset. The camera is pointed at a declination of 90° and a frame is taken, the camera is then rotated by 2hrs between each image. When observing a target, a 120s exposure image is taken, first in the visual filter, then again in the red and infrared. The sequence is then repeated seven more times so a total of 24 images are taken, with eight in each filter. The whole process takes around an hour.

Efforts are made to observe all the clusters as often as possible. However, multiple factors can prevent daily observations. Weather is a large factor; cloud and rain mean the telescope cannot be used. Strong wind and high humidity can severely reduce image quality. Even on clear nights not all objects can be observed; some months objects are too low, or below the horizon. In the summer months there are not enough hours dark

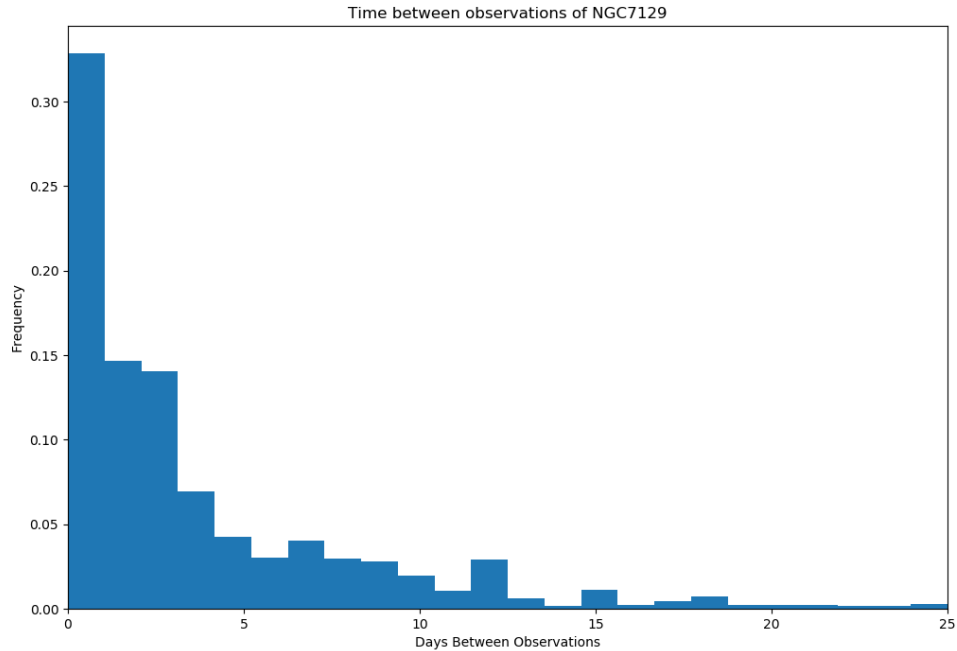


Figure 3.1: *Histogram of distribution of cadence between observation for target NGC7129*

enough to observe all available objects.

The majority of targets have a most common cadence of a single day, as seen in figures 3.1 and 3.2; histograms of the cadence distribution of NGC7129 and IC5070. The targets are most frequently observed objects in the project; NGC7129 as it is always within a viewable position, and IC5070 due to the interesting activity of objects in the nebula. IC1396A breaks the trend with a most frequent cadence of 3 days between observations. While not as frequently observed as other objects, the frequency of cadences longer than 3 days is lower than the frequency of shorter cadences as seen in figure 3.3 (cadence values and graphs courtesy of J.K.Crumpton). The total collected data used in this project ranges from September 2015 through to November 2017, a span of a little over 2 years.

All data analysis, such as making plots, finding dips and calculating the disks' physical

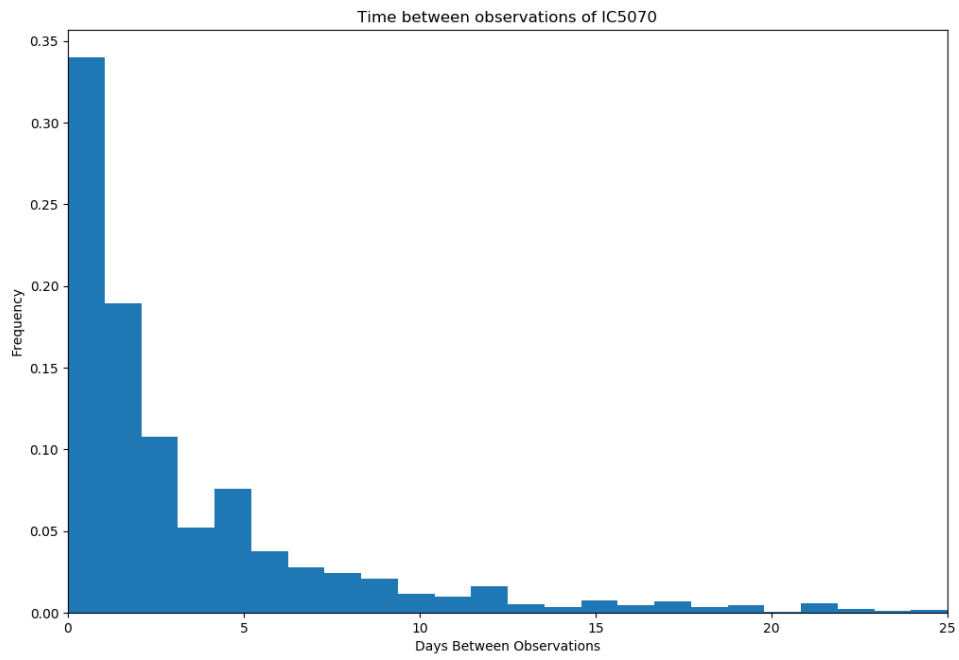


Figure 3.2: *Histogram of distribution of cadence between observation for target IC5070*

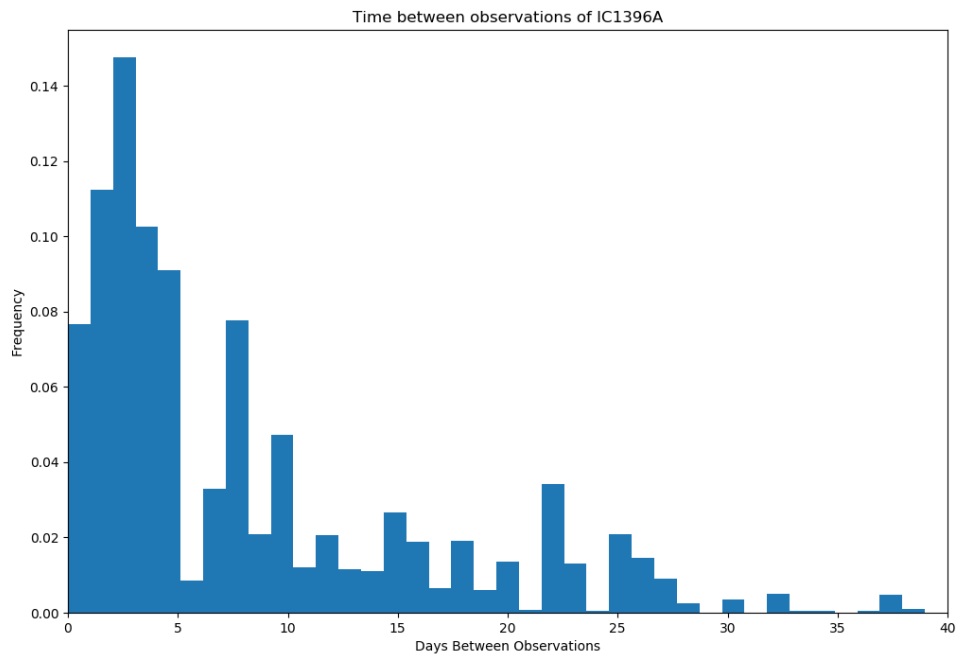


Figure 3.3: *Histogram of distribution of cadence between observation for target IC1396A*

properties, was done using python. The initial light-curve data consisted of the Julian date, full date and time, and the magnitude for each of the three filters. The values of the visual magnitude, minus the infra-red magnitude was also included.

3.2 Defining a Dip

YSOs often display variability in their magnitude, most often this variability is the result of a slow process such as a change in radius or accretion rate. This variability can make the detection of dips from occultations difficult to spot, especially if they occur during a longer term dip. To combat this, a running median filter is applied to the data from a light-curve before analysis. This is done by selecting a point in the curve, and every point 100 days either side:

$$((t > t[i] - 100) \quad \& \quad (t < t[i] + 100)) \quad (3.1)$$

Where t is the Julian date, and $t[i]$ is the Julian Date value of the selected data point. The median magnitude (M) of the selected points is then found, and the value assigned to the original data point as a comparison value. This is done for every data point in a light curve.

This results in a 'smoothed' light-curve, essentially flattening the long term fluctuation of the star, while leaving the short, strong dips in magnitude visible. A dip can only be detected if it is notably shorter than the width of the filter used on the light-curve. A filter width of 100 days was chosen to prevent larger dips from being missed while still suitably smoothing the curve. As an individual star's magnitude can fluctuate at different rates, the fixed filter width will not have been the most suitable width for every object in this study. This means shorter, more shallow dips may not be noticed in light-curves with frequent fluctuations. This complicates attempts to get a program to calculate the most ideal filter length for each curve individually.

The data points were sorted by whether or not they were part of a dip through sigma clipping (eq 3.2). The median magnitude of the flattened curve was found along with the standard deviation (σ). Any point more than 3σ fainter or brighter than the median was

considered to be in a dip. These points are 'removed' as the loop restarts, finding the new standard deviation while ignoring these points. Before again, finding which points are more than 3σ from the new median. This loop continues until the change in standard deviation between two cycles is less than 0.1%.

$$\frac{\sigma_{previous} - \sigma_{new}}{\sigma_{new}} < 0.001 \quad (3.2)$$

Assuming every object has gaussian noise, using 3σ as a limit means 99.7% of points not in a dip should be recorded. However, statistically, 3 in 1000 points could be recorded as part of a dip when they are not. Across all the targets a total of around 46,000 data points were recorded, therefore, statistically 138 points are expected to be falsely recorded as dips. To avoid this uncertainty, dips containing a single data point were ignored during data analysis. While this reduces the chance of anomalous results, there is also a risk of shorter dips being ignored; something a shorter cadence between observations could potentially rectify.

Once the dips of a curve have been identified, they can be analysed to find their depth, duration, and area. These values can then be used to estimate the physical properties of the material in the circumstellar disk, such as its radius and mass. Patterns in the occurrence of dips such as similar dips appearing at regular intervals, are indicative of a fixed orbiting body or other system, for example, a binary system.

3.3 Measuring Dip Properties

When calculating any properties of material, it was assumed that the material was perfectly spherical in shape, with a constant density. In reality, clouds of interstellar material are irregularly shaped, and when planets are being formed their cores will be denser than the surrounding material

The depth of a dip can provide information it would give on the size and density of material around the star; the drop in magnitude will be proportional to the amount of

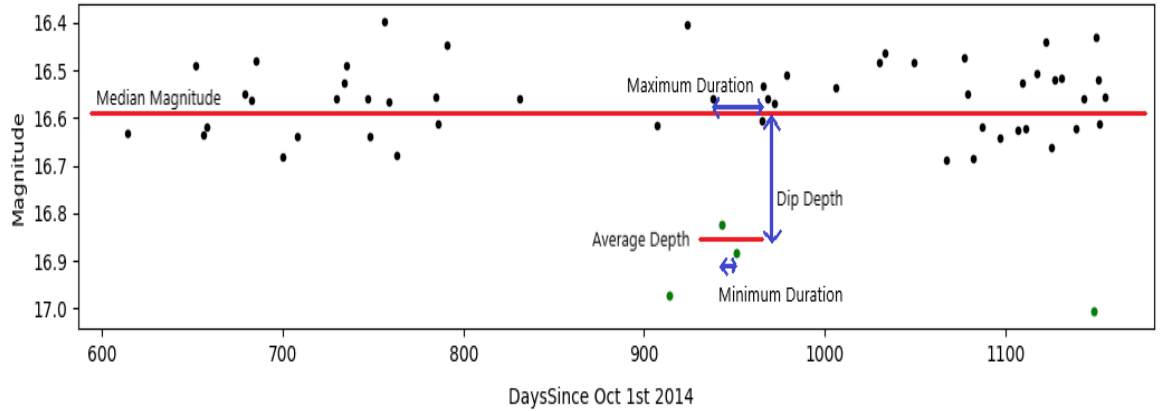


Figure 3.4: *Diagram of an example lightcurve showing the dip parameters measured. These are: maximum duration; time difference in days between two data points either side of a dip, minimum duration; time difference in days between the first and last points in a dip, and dip depth; the magnitude difference between the median magnitude, and the average magnitude of the points in a dip*

material in front of the star along our line of sight. To measure the depth, the median magnitude of data points in the dip was found, and the median value of the flattened curve subtracted. Median magnitude was used to give a single value for depth, in order to simplify later calculations of radius and mass. The magnitude varies between points in a dip. The shape of a dip is indicative of an object's change in density and shape. These properties are not automatically noted by the python code used.

The duration of a dip allows for the calculation of the radius of the material passing in front of the star. Two values were recorded; the minimum and maximum duration. As previously mentioned, clusters are not observed every night for a variety of reasons and even when they are, clusters are only observed once a night for a period of one hour. This limits the chance of observing an object precisely as a dip starts or finishes. Therefore, the minimum duration was defined as the time between the first and last data points in a single dip. The maximum being the time difference between the data points within the median magnitude of the star, directly either side of a dip.

This leaves a non-constant uncertainty for the duration between every dip for each object arising from irregular observations of the targets. Assuming a dip starts and ends exactly in the middle between the minimum and maximum duration points, the range of uncertainty can be said to be half the average difference between the maximum and minimum duration. All calculations using the duration were initially completed twice; once using the minimum duration, and once using the maximum duration. This was done in case of a significant difference in the results. As a result, while specific values varied, the overall trend of results for both the minimum and maximum duration followed the same logarithmic distribution pattern, as can be seen in figure 3.5. This allowed the average of the two values to be used as a reliable estimate for dip duration to be used in further calculations. To have a truly exact value for dip duration, an object would have to be observed as frequently as every few hours. This would require a network of telescopes to allow constant observation of a target.

The time difference between the centre of one dip to the centre of the next was calculated. If this value was taken for every dip in a lightcurve, and the values used to make a histogram, a peak on the histogram could be indicative of an object regularly orbiting around the star. The lightcurve would have to be checked to make sure this peak in frequency coincides with dips of equal depth and duration to each other. Few of the observed objects showed sign of a regular orbital period. However, it is possible that with more data, more orbital patterns would be observed. Knowing the time difference between dips can give an indication of when to focus observations on particular clusters. More data points in a dip would produce a more detailed curve. Which would provide more information on its exact duration, and how the mass of the material varies throughout.

Finding the area of a dip could give insight to the distribution of material in gas and dust clouds. The trapezium rule was used to find the area. The trapezium rule is defined as:

$$\int_{x_0}^{x_n} F(x)dx = \frac{1}{2}h[(y_0 + y_n) + 2(y_1 + y_2 + \dots + y_{n-1})] \quad (3.3)$$

and is a method of estimating integrals of area under a curve. It works by finding the area under a curve between two data points by treating the points as vertices of a regular trapezium. For the area of dips, the median value of the flattened curve was used as a

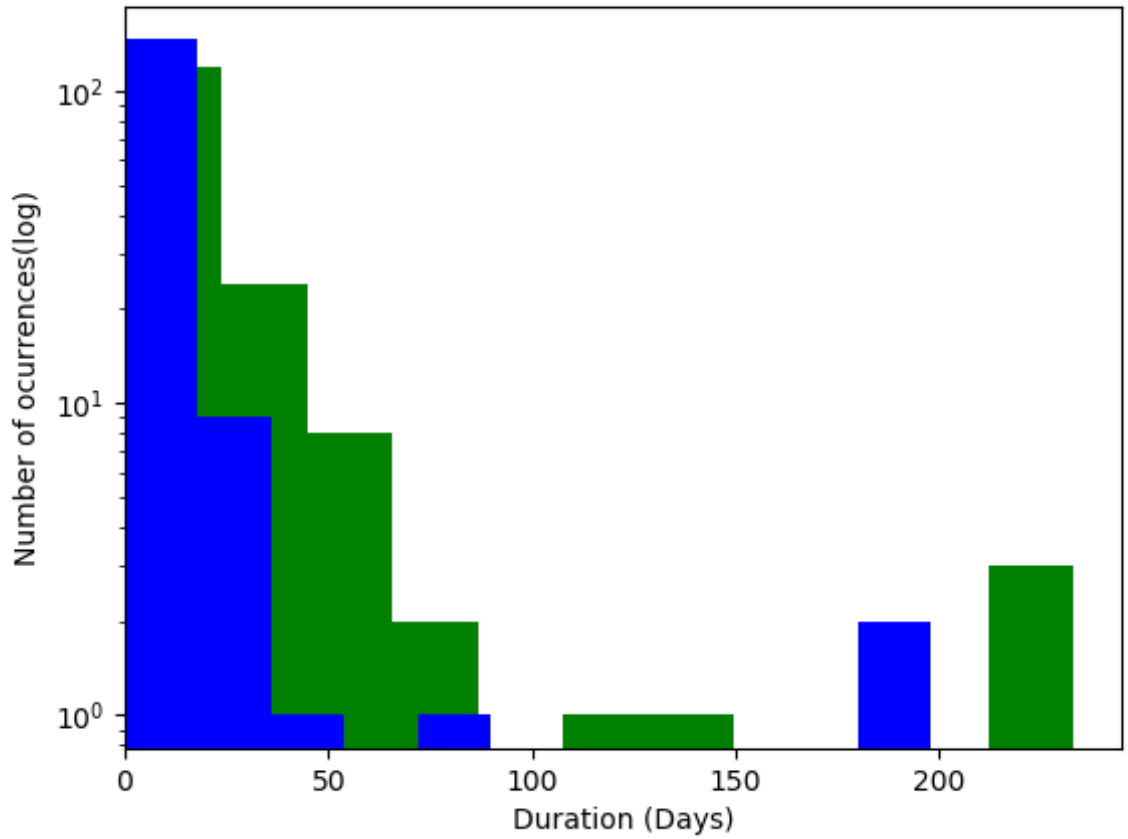


Figure 3.5: *Histogram of the distribution of both the minimum and maximum durations for all analysed. The minimum duration is shown in blue, and the maximum duration in green.*

base axis, with the change in magnitude being used as y values, with the Julian date for x values. The value of h was calculated between each data point as the change in Julian date. Using the trapezium rule meant the area could be accurately found while still considering the shape of the dip.

3.4 Calculating Radius and Mass

The dimension (R) of the material was found by multiplying velocity and time together to find the distance covered by material in the time frame of the dip. With the duration of a dip being used as time, velocity had to be calculated. Velocity was found by equating the centripetal and gravitational force formulas, and rearranging for velocity.

$$F = m \frac{v^2}{r} \quad (3.4)$$

$$F = \frac{GMm}{r^2} \quad (3.5)$$

Equating equations 3.4 and 3.5 and rearranging for velocity gives equation 3.6.

$$v = \sqrt{\frac{GM}{r}} \quad (3.6)$$

(ms⁻²)

Calculating velocity calls for values of the mass of the stellar object, and the distance from the star to the material in the disk. As these values are not explicitly known, assumptions were made for all objects in the study. The star was assumed to have a mass (M) of 1 M_⊙. The material is assumed to lie 0.4Au while material in the disk will vary greatly, 0.4Au was assumed as it would be comfortably within the inner disk of a young object, it is within the inner disk that the most activity could be expected in young objects. The calculated values would give a rough idea of the size of clouds of material. However, it can be assumed that not all the material would be at the same distance from the star. Material closer or further from the star would have different radii to what is calculated.

Most of the objects observed are young enough that the accretion disks contain mostly small dust particles. Therefore, the material was treated the same way as interstellar

clouds. The first step was to work out the number of hydrogen particles per m² column using equation 3.7.

$$N(H) = 6.8 \times 10^{26} \frac{A_v}{R_v} \text{ (Bohlin, Savage, And Drake, 1978)} \quad (3.7)$$

Where 6.8×10^{26} is the number of hydrogen particles per m², A_v is the drop in magnitude of the light-curve, and R_v is the total to selective extinction ratio, which regarding the average age of the targets, is assumed to be 3.1. Multiplying this value by the mass of a single hydrogen particle (1.67×10^{-27} kg) gives the mass of the column ($M(H)$). This leaves the density (ρ) to be found by dividing $M(H)$ by R .

$$\rho_{[kgm^{-3}]} = \frac{M(H)}{R} \quad (3.8)$$

Once the density has been calculated, it can be used to find the mass of a sphere using a radius with the value of the calculated dimensions of material.

$$M_{[kg]} = \rho \times \frac{4}{3} \times \pi \times R^3 \quad (3.9)$$

This gives an estimate mass for the clumps of material in the accretion disk. It is unlikely the material has genuinely formed perfect spheres all at the fixed distance from the star. However, current data and calculations can be used in further study to find a more accurate model for the accretion disks of these objects. For the presentation of data, the mass of material in the accretion disk was converted in to lunar masses (1 Lunar mass = 7.35×10^{22} kg).

3.5 Material density and dust growth

To determine the nature of the material in the circumstellar disk, the magnitudes of an object in both the visual (V) and infra-red (I) filters were used. For every data point, the value of the visual magnitude, minus the infra-red magnitude (V-I) was calculated. For each object, the V magnitude value of every data point classified as being in a dip was

plotted against the V-I value for that data point (an example plot can be seen in figure 3.6). The gradient of the plot was then found to give a value of α (equation 3.10).

$$\alpha = \frac{\Delta V}{\Delta(V - I)} \quad (3.10)$$

This arc tangent value for α was found in radians, and then converted into degrees. The final value is indicative of the material around the star, with 45° being equivalent to noise from the visual data, and 65° being a typical value for interstellar dust emission.

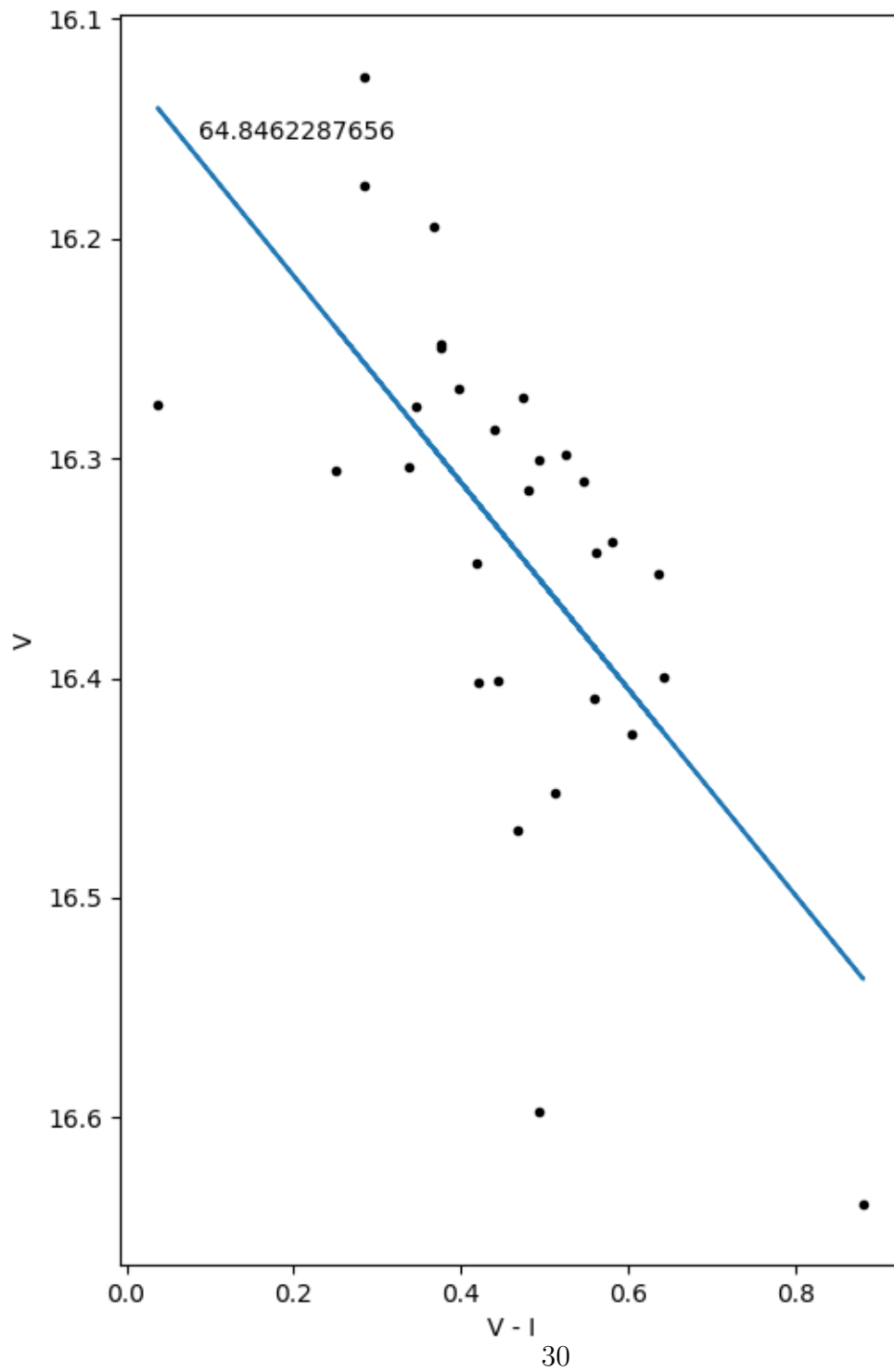


Figure 3.6: An example v against $V-I$ plot

Chapter 4

Results

4.1 Identifying Dips

4.1.1 Single Data Point Dips

Across the eight observation targets, light-curve data was collected for a total of 819 individual objects. All of these objects have data regularly collected as part of the HOYS-cAPS project. Of these objects, 466 are variable, with output in the V band varying by at least 0.2 Mag, with 413 objects confirmed to be YSOs younger than 10 Myr (Froebrich et al., 2018a). The total number of data points recorded for all objects, including non-variable stars, was approximately 46,000. Targets such as IC348, NGC2244, and NGC1333 are less well observed, with more sparse light-curves that may only contain between 30 and 50 data points. Other, more frequently observed targets include IC5070 and NGC7129 with upwards of 150 data points per light-curve. From this data, 1395 dips were found, including dips containing a single data point. A non-variable object from the observation targets will only produce dip data if noise from the star is recorded to be more than 3σ from the median magnitude of the object as discussed in Section 3.2. The presence of some older objects with variable magnitude may disrupt the data, with older variable objects

making up 11% of the sample that will provide dip data. Some data from these objects will be removed along with the single data point dips. For dips of multiple data points; older objects are more likely to have further developed planetary systems the material orbiting them will be larger, and of higher density, causing outliers in dip analysis data from predominantly with smaller, less dense clumps of material orbiting them.

Dips containing single data points were removed before analysis to remove noise errors. This left 159 dips for analysis, removing a total of 1,236 dips, a much greater value than the 138 dips expected, due to calculations mentioned in section 3.2. While it would be expected to have more single points recorded than the noise calculations may have suggested due to the existence of additional outliers, some of this discrepancy could likely be caused by legitimate dips being removed from analysis due to objects only being observed once during dips. Another contribution to the large number of removed dips may be the presence of dips from changes in accretion rate to a star. Being short term magnitude changes, they would have intentionally not been filtered out of the curve.

Part of the definition of a dipper star is that its dips in magnitude are very short, sometimes only a few hours long. This fact is likely the main contribution to the number of dips not being included in the analysis being so much greater than the expected number of false dips due to noise. With a single telescope available to observe 8 targets as frequently as possible, it is not always ideal to perform observations for a single target multiple times a night. As such, the minimum cadence for observations of any of the targets is one day. This takes away the ability to observe dips only a few hours in length more than once during each dip, and so the dips from these objects would have been unnecessarily removed from the dip analysis. Even dips that are a few days in length may only be observed once during the dip as objects are not necessarily observed daily. IC1396A for example, has a most common cadence of 3 days, and an average cadence, per 30 days, of 7 days. Dependent on the time, a dip starts in relation to the times of observation; a dip lasting several days may still only be observed once.

It is also possible for an object to be observed on multiple occasions during a single dip, but for only one of the data points to have a faint enough magnitude relative to

the object's median magnitude to be recorded as part of a dip. This is possible for occultations by clumps of material of inconsistent density, perhaps with a dense core surrounded by less dense material. For some objects, these less faint data points may be missed if an inappropriate filter width has been used to flatten the light-curve, resulting in more scatter in the flattened curve. This scatter may result in a more faint value for the median magnitude of the star. As a result, the program would only be able to detect the absolute faintest data points in the dips. While reducing the proportional magnitude change required for a data point to register as part of a dip would allow less faint points to register, to apply this change to the entire curve would increase the number of falsely recorded dips as a result of noise in the star. However, to apply these looser criteria to just the points either side of a dip could show an increase in the number of multi data point dips.

An example of single data point dips that could potentially include more data points is shown in figure 4.1. In this plot the magnitude of the visual output of the star is mainly recorded as being between 15Mag and around 15.75Mag with a few notably fainter points, down to nearly 17Mag. At around 950 since October 1st 2014 there are 2 single data point dips separated by a single non-dip data point. The separating point is more faint than the data points either side of the two single data point dips and is one of the faintest points not classified as part of a dip. While it is possible this is a case of two, separate, small dips, this could also be an example of a curve that would benefit from an adjustment in the criteria of defining a point as part of a dip.

4.1.2 Effect of filter width of dip detection

For some objects, the filter width of 100 days either side of a data point, was so unsuitable that it prevented dips being detected altogether. Objects with very long term fluctuations remain unchanged when passed through the 100 day filter as is seen with GM Cep in IC1396A in figure 4.2. The similarity between the middle and bottom panel of this figure shows how unsuitable a filter of 100 days is for this object, so much so that none of the extremely faint points towards the end of the recorded lightcurve are detected to be part

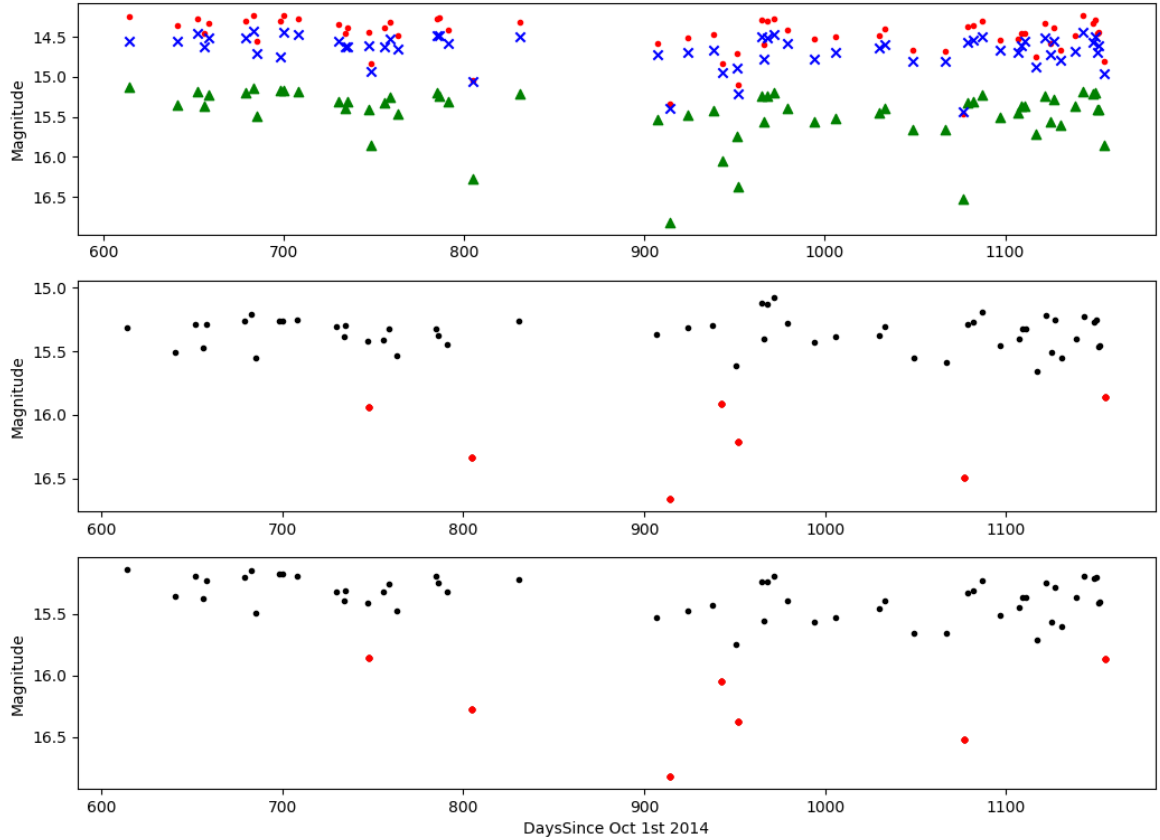


Figure 4.1: *Light-curve for object J21371591 in cluster IC1396A. The top curve shows the magnitude of the star in the 3 filters used to record data, green represents the visual filter, red represents the red filter, and blue shows the infra-red filter. The middle plot shows the flattened light-curve in the visual filter, with data points in dips highlighted in red. The final plot shows the original light-curve with dips also highlighted in red.*

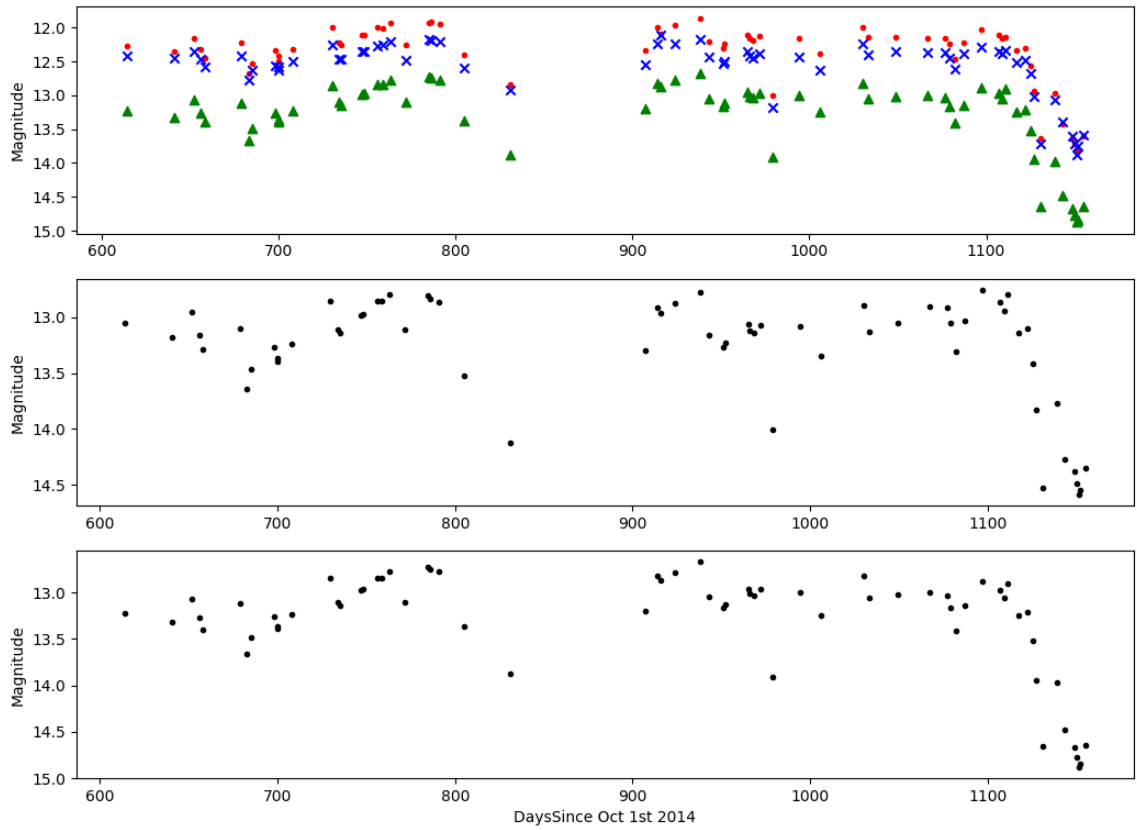


Figure 4.2: *Light-curve for the object GM Cep, in the cluster IC1396A. The top, middle, and bottom plots showing the full light-curve in all 3 filters that magnitude was recorded in, the filtered light-curve in the visual filter, and the original light-curve in the visual filter respectively*

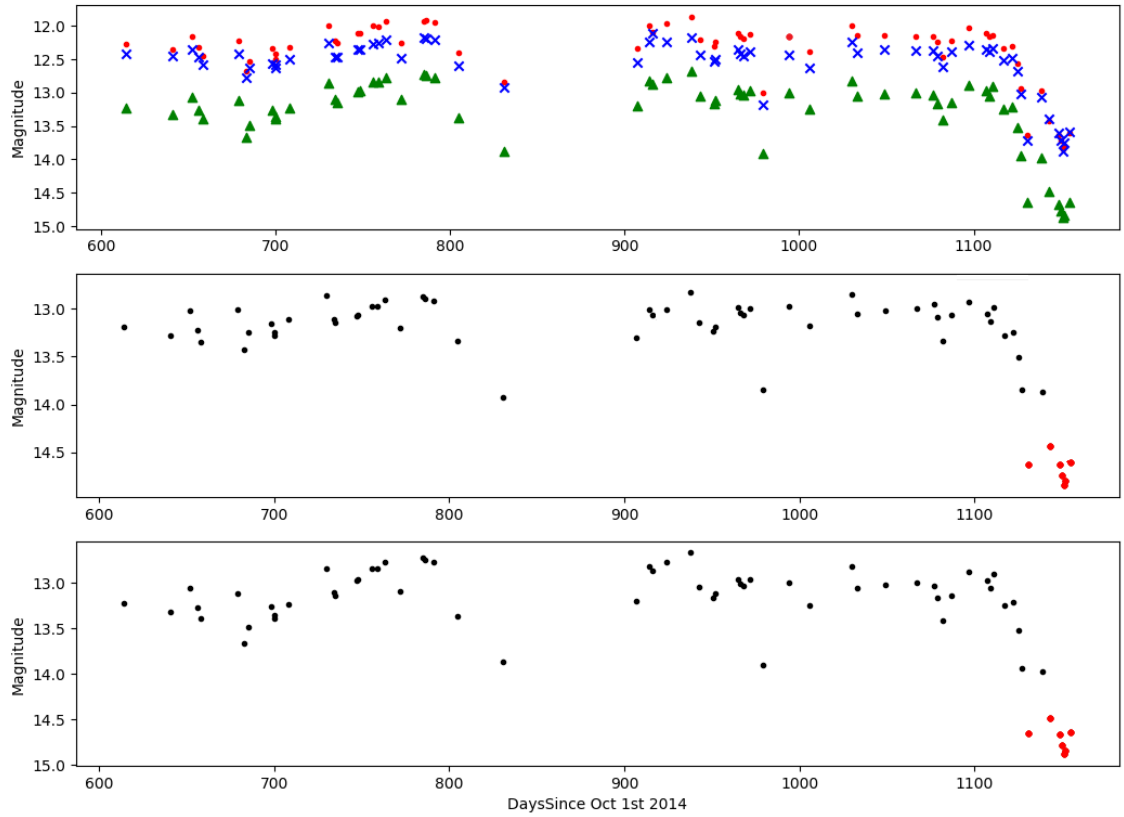


Figure 4.3: *Light-curve for the object GM Cep in the cluster IC1396A with a smoothing filter of 250 days. The top, middle, and bottom plots showing the full light-curve in all 3 filters that magnitude was recorded in, the flattened light-curve in the visual filter, and the original light-curve in the visual filter respectively. All dips are highlighted in red.*

of a dip, despite being much fainter than the other points of the curve. What can also be seen in this lightcurve, is a sinusoidal pattern with a period of around 200 days. Figure 4.3 shows the same objects after being filtered using a 250 day filter. The sinusoidal pattern seen in the original curve is less noticeable in the middle panel, and the significantly fainter points towards the end of the observed curve are now highlighted as being a dip, showing that this longer filter is more appropriate for this curve, than the 100 day filter used for the analysis. A more recent plot of the data for this object can be seen in figure 4.4, which includes data from Julian date 2457839 (900 days since Oct 1st 2014) up to September 2018. This plot shows that the large dip seen towards the end of the light-curve in figure 4.3 lasts for around 130 days, a similar duration to the previous large drop in magnitude, where the star became too faint to observe. It is unlikely that these large dips were caused by material in the inner disk. There are smaller dips within the star's sinusoidal fluctuation that go undetected, meaning potential activity of the inner disk is not being observed.

There are also examples of the 100 day filter width being too wide for objects with more frequent fluctuations in magnitude. This can be seen in the light-curve for the object J03444011 in the IC148 cluster shown in figure 4.5 where it is apparent the 100 day filter has not sufficiently flattened the light curve to find all data points in dips. There are large gaps in observations where the cluster is not visible for parts of the year, and where there are observations, there is a large amount of scatter in the stars magnitude. The wide filter includes too many data points for the variations to successfully cancel out. Figure 4.6 shows the same object using a filter width of 50 days. This time two dips of single data points were detected, and there is a visible difference between the curves in the 2 lower plots. This suggests that the object may be a dipper star, and with more investigation into a suitable filter width, the dips could be analysed for information on the star's inner disk structure. These dips were found separately from the rest of the sample, and were therefore not included in dip analysis.

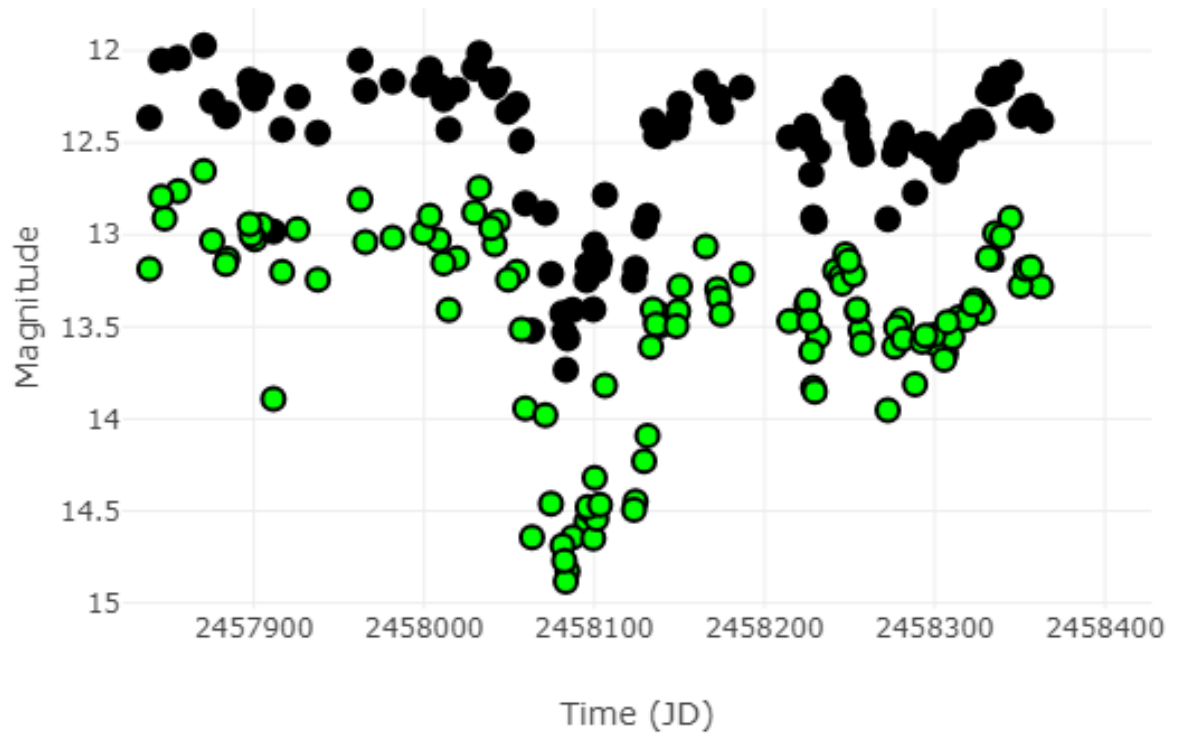


Figure 4.4: *Light-curve for GM Cep from April 2016 to present (September 2018). The data from the visual filter is displayed in green, and the infra-red data displayed in black.*

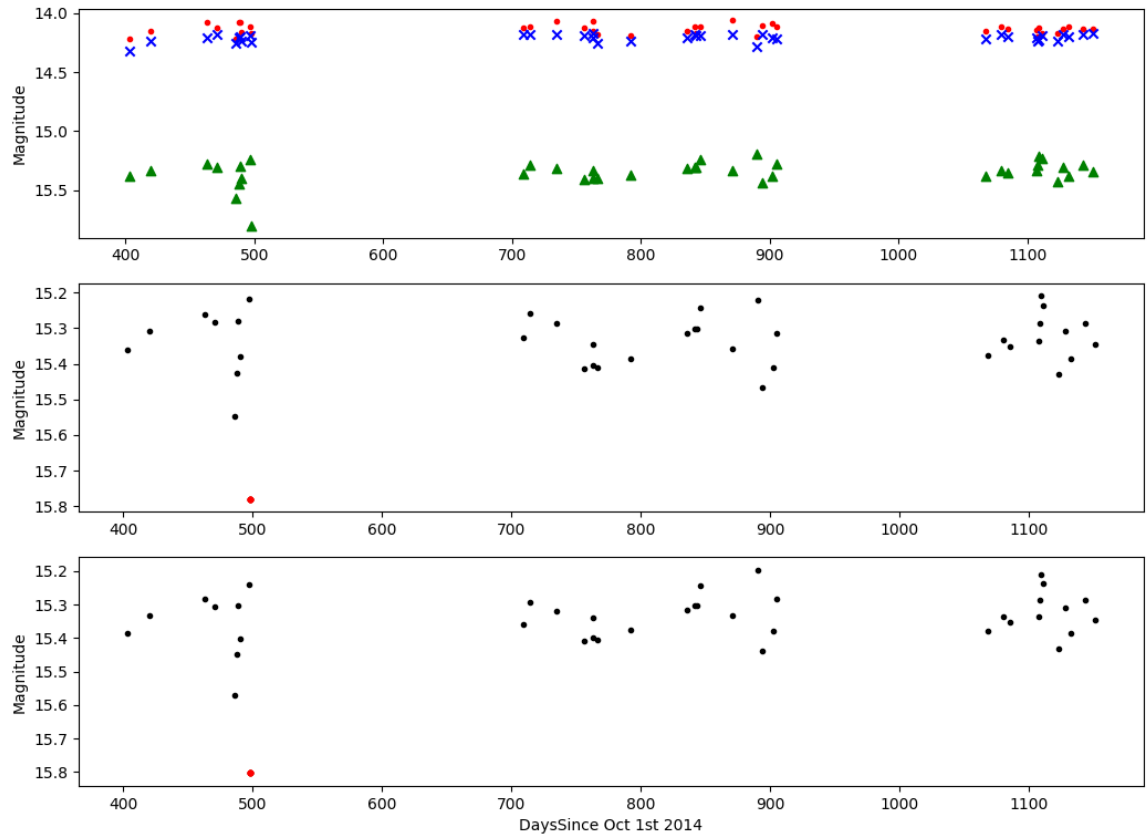


Figure 4.5: *Light-curves for object J03444011 in cluster IC148*

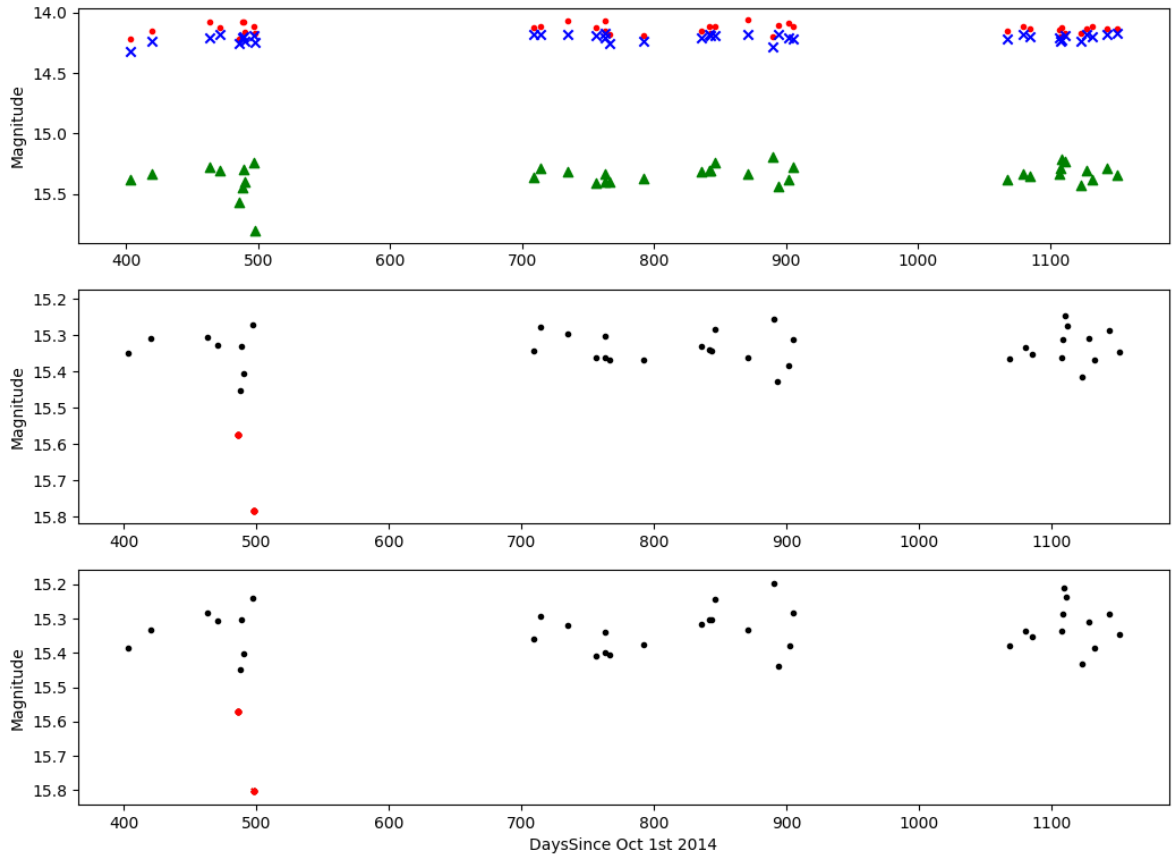


Figure 4.6: *Light-curves of object J03444011 in cluster IC148 with a 50 day filter width*

4.2 Dip Depth

The depth of a dip is indicative of changes in the column density of the material present in the disk along our line of sight. Figure 4.7 shows the distribution of dip depths across all analysed data. The distribution in this figure matches the depth distribution in Hedges, Hodgkin, and Kennedy (2018), where the data collected was displayed alongside data from Ansdell et al. (2016b). The consistency in depth distribution to these papers proves the success in correctly identifying dipper stars and their drops in magnitude caused by occultations from their inner disks. It also shows consistency in the behaviour and activity of the inner circumstellar disk across a range of YSOs.

The data for the dip depth appears to follow an inverse power law distribution, especially visible in dip depths greater than 0.25mag. This is as expected, as the disk at a young stage will consist mostly of fine dust and gas. While increased densities of this material can clearly cause dips in magnitude, it is unlikely that clumps of material large, or dense enough to cause extreme dips in magnitude will occur as regularly as smaller, less dense clumps. This is particularly relevant in the inner disk where fast moving material would lead to frequent shifts and changes in material density. The lower count of dips with depth less than 0.2mag may in part be due to the fewer occurrences of clumps of material with low column density that is still sufficient to cause a drop in magnitude. Shallow dips are also less distinguishable from noise, particularly if a star displays a large amount of noise. As such, it is expected for there to be fewer recorded dips of depth less than 0.2mag. All objects will have noise and so, detecting dips as shallow as 0.1mag or less is extremely unlikely.

4.3 Duration

The duration of a dip relates to the radius of the material causing the dip, when taken in conjunction with dip depth, a value for material density can be calculated. Magnitude dips of dipper stars typically last from hours, up to several days. For the purpose of this

thesis longer dips lasting multiple weeks were still considered for dipping stars as these dips may give insight to the structure of a circumstellar disk beyond a distance of 1AU from the star. These will be useful in future work when investigating the structure of circumstellar disks in their entirety.

As briefly mentioned in section 3.3, both the minimum and maximum duration were measured with similar distribution patterns. The distribution of the maximum duration (shown in figure 3.5) appears to follow a more shallow power law distribution compared to the minimum duration. This is likely due to the varying interval between observations, which can cause dramatic differences between the minimum and maximum duration for a dip. Longer dips appear to be more affected by this; as seen with the distribution peak seen at around 100 days. With a peak visible around the same point for both values, it is possible to assume that they are related to the same dips. Despite this, there is a difference of over 50 days between the two duration values, making an accurate value for the average duration difficult to determine. The distribution of minimum and maximum duration was similar enough to allow the use of the average duration for future calculations such as the radius of material clump in the disk. The potential overestimation of the dip duration should be taken into account when observing results such as the radius of material in the disk, for which the only variable in the calculation is the dip duration.

Figure 4.8 shows the average duration of every dip analysed. As was the case with dip depth, the distribution in this figure is similar to the dip duration distribution seen in Hedges, Hodgkin, and Kennedy (2018) except with the inclusion of longer dips. The longer dip durations are likely seen due to there being no maximum dip length for analysis, as well as taking the average dip duration regardless of the cadence between observations. Figure 4.9 shows the duration distribution for all analysed dips with a duration of 30 days or less, which includes around 150 dips, the vast majority of dips analysed. The logarithmic y-axis has been changed to allow easier comparison to Hedges, Hodgkin, and Kennedy (2018). The distribution of the duration of these shorter dips is still similar to that seen in the work by Hedges, Hodgkin, and Kennedy (2018), although the power law followed in figure 4.9 appears to be shallower. This could be the result of taking the duration average or from including different observation targets.

Most of the dips recorded and analysed fell comfortably within the expected length of dips seen around dipper stars. It is clear from figure 4.8 that apart from small peaks at a little over 100 days and around 200 days, the vast majority of dips lasted no more than 50 days. Of that majority, the highest frequency of dips is seen to be between around two and three days, up to roughly 30 days. While the frequency of these short dips can be used to predict the structure of material in the inner disk, the longer dips give information on disk structure at greater distances from the central star, assuming the dips are caused by occultation of material. It is unreasonable to assume that material in the inner disk could cause a dip in magnitude lasting 200 days consistent with the peak in figure 4.8. The dip may have instead been caused by slower moving material in the outer disk. Further investigation of these specific dips, such as noting the depth of the dips, and how the magnitude changes throughout the dip, can provide information on the structure of the material present. A shallow dip with a near semi-circle shape may suggest a spherical cloud of dust of constant density. The work of Bouvier et al. (2003) suggests this change in magnitude is likely caused by disk warps due to magnetic field lines. There is potential that a recurring dip of this length, with a more intense drop in magnitude in the centre of the dip, may indicate planet formation and a protoplanetary disk although, this is more likely to be seen in disks around older objects.

4.4 Material Dimensions

The calculation of dimensions assumed that all dips were caused by material within the inner disk, spherical in shape, and at a fixed distance of 0.4AU from the central star. With this assumption, the only variable in the calculations was the duration of the dip. Therefore the distribution of the size of material will be the same as the distribution for duration. With the presence of dips longer than 25 days, some of the calculated dimensions for material in the disk are upwards of 6AU, as can be seen in figure 4.10. While these are completely unreasonable values for material so close to the star, this flaw should have been considered when simplifying all the material to a consistent distance quite so close to the star. Material in the outer disk that may have caused the long dips which gave

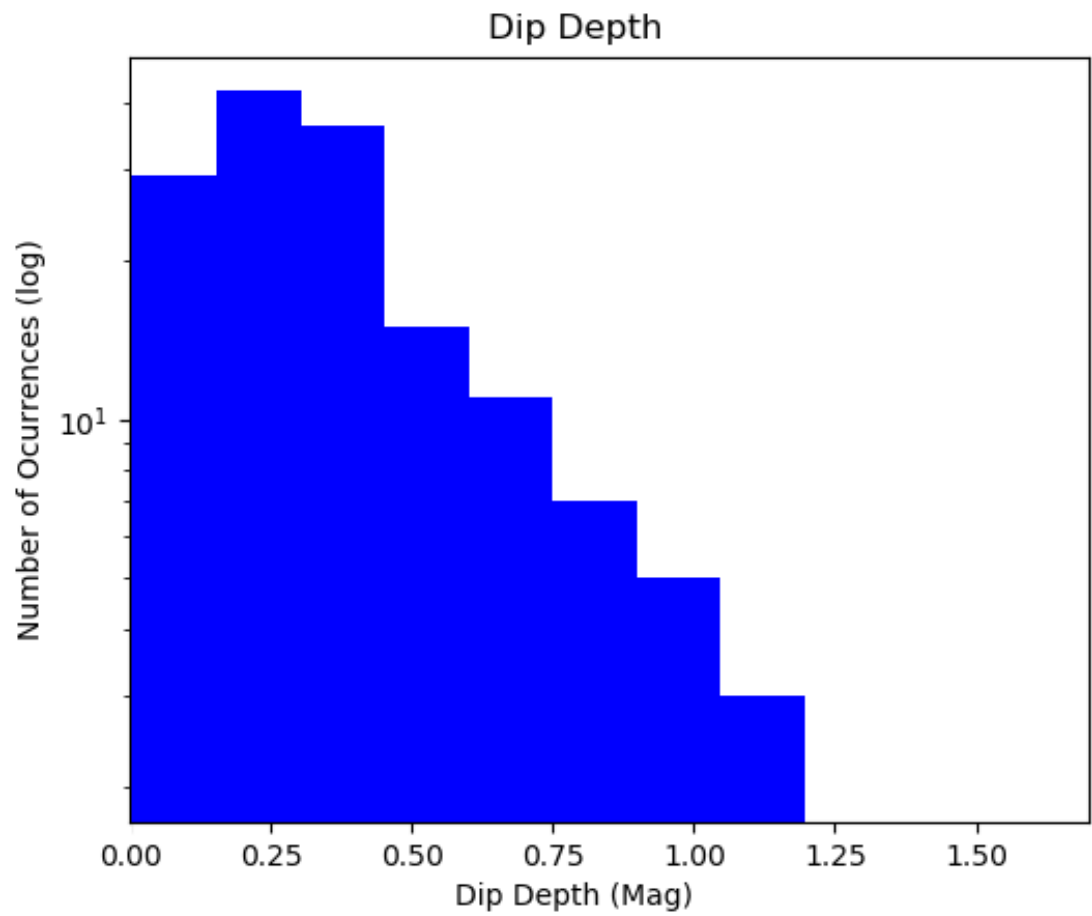


Figure 4.7: *Histogram of the distribution of the dip depth for every dip analysed with a logarithmic y axis*

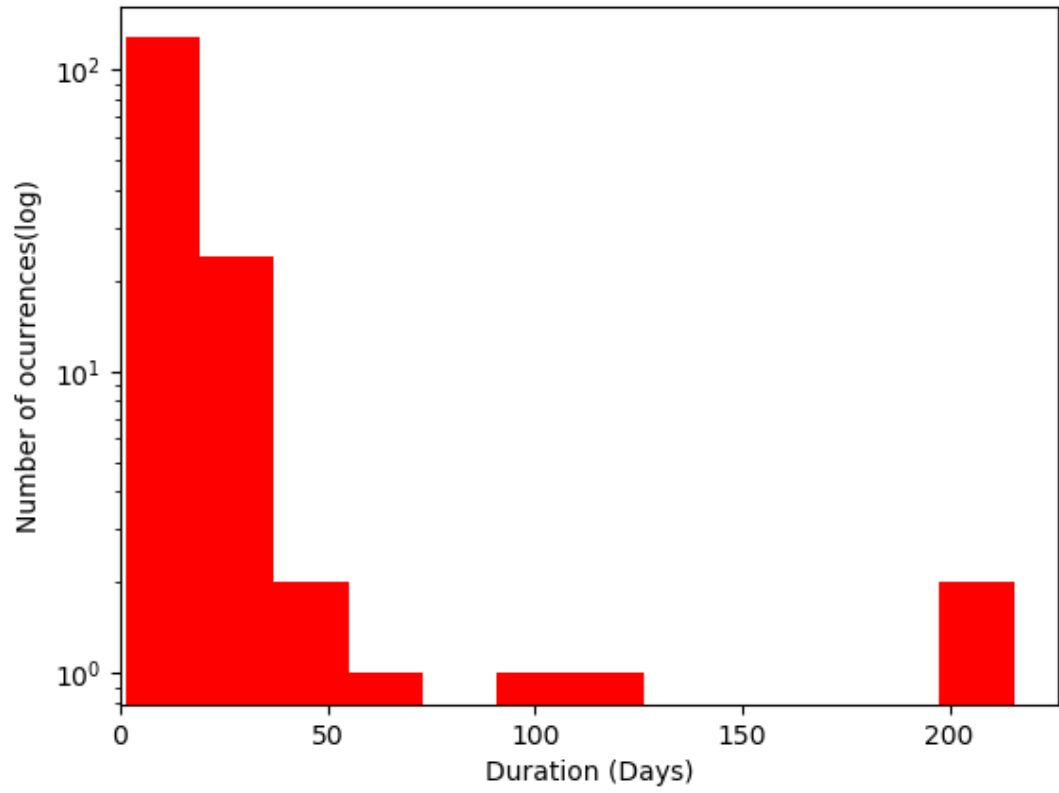


Figure 4.8: *Histogram of the distribution of the average duration for every dip analysed with a logarithmic y axis*

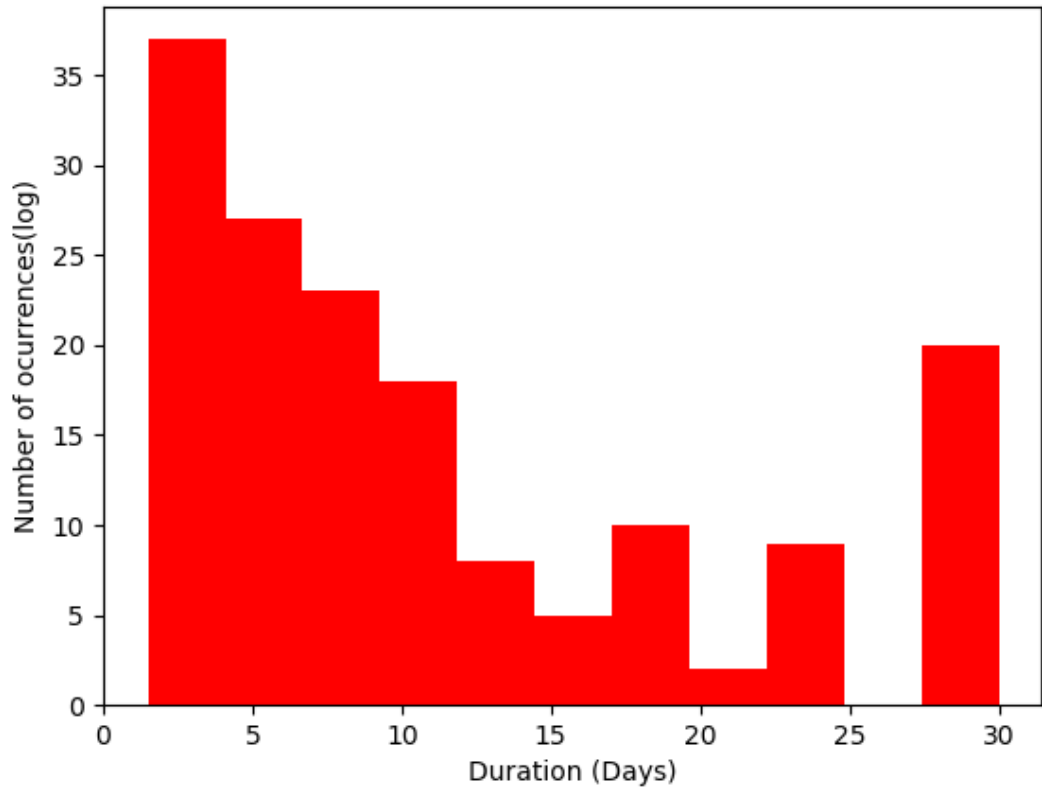


Figure 4.9: *Histogram of the distribution of average dip duration for all analysed dips shorter than 30 days*

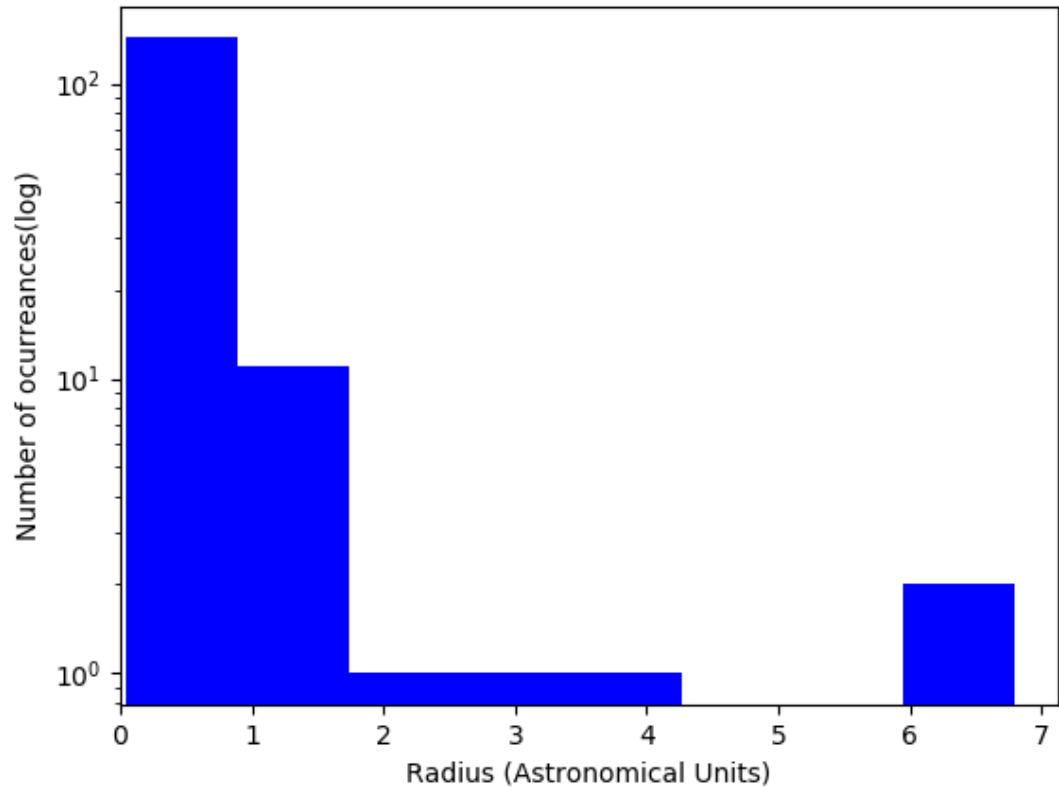


Figure 4.10: *Histogram of the distribution of the estimate dimensions of material calculated for every dip analysed*

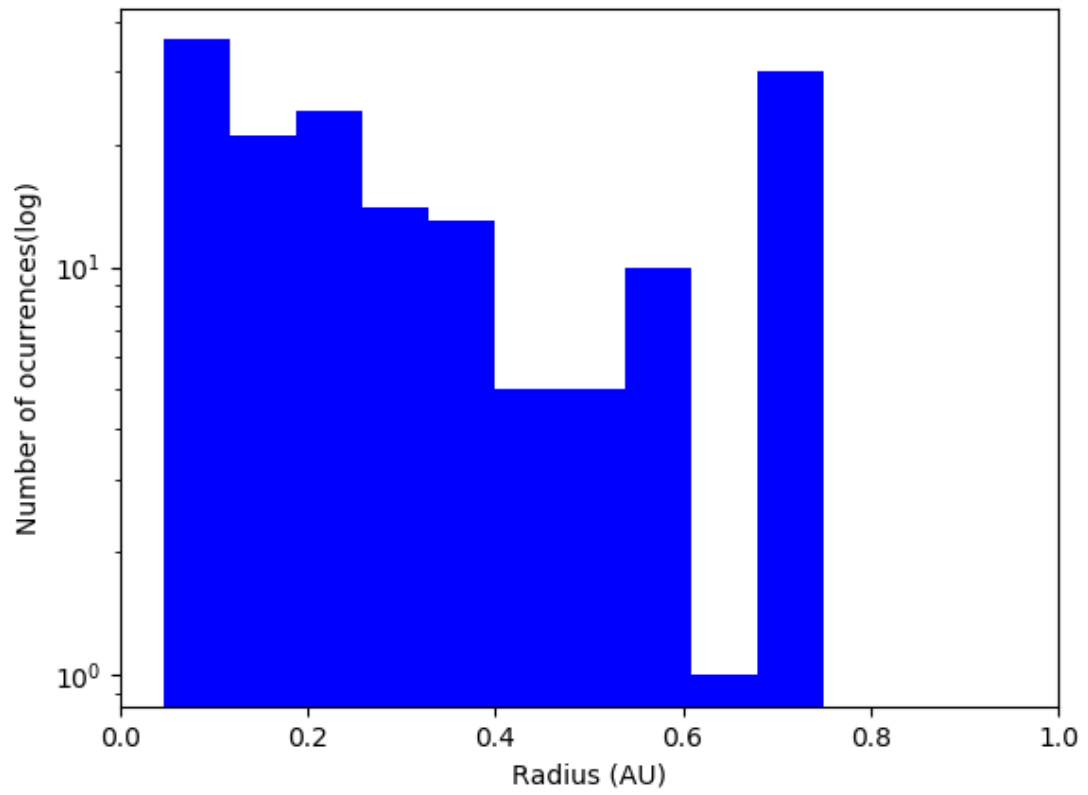


Figure 4.11: *Histogram of the distribution of dimensions less than 0.75AU.*

this value considering the calculations would have used the velocity of the fast moving material in the inner disk. The estimate velocity would have been too high, which would have resulted in a higher value for the dimensions. In reality, material in the outer disk would still be much smaller in size than 6AU. The longer duration dips may also not be valid, and so to avoid analysing inaccurate, or potentially invalid results, the focus will be on the distribution of size values less than 0.75AU. While this is significantly greater than the assumed 0.4AU distance, it will include the portion of results calculated from the 135 dips less than 25 days long.

The distribution of dimensions below 0.75AU, shown in figure 4.11, appears to follow a similar pattern to the distribution of the average duration for dips shorter than 25 days. Over 100 of the 159 dips analysed have a dimensions value below the assumed distance of 0.4 AU from the star, of these 70 gave a radius of 0.25AU or less. This could suggest that a reasonable number of the dips analysed were caused by clumps of material very close to their respective object

There are fewer occurrences of dimensions above 0.4AU, but still a significant portion of the analysed sample. The most likely cause of this is clumps of more dense material at greater distances from the star than 0.4AU. By observing the time difference between consecutive dips, it is possible to determine if there is a periodic pattern in the dips for that star. If this is the case, a more accurate distance between the material causing the repetitive dips can be calculated, which then allows for a more accurate calculation of the size and mass of the material.

It is possible for some of the dips that give dimensions values over 0.4AU to be caused by channels of material around the star. Channels occur when material in the inner disk is forced into rotating channels which spiral towards the star, allowing the accretion of material to the central star. If these channels have a higher column density than the rest of the material in the disk, they will show up as dips when passing along the line of sight. If the channel spiralling around the star remains along the line of sight as the star rotates, it will cause a long dip. This is a good illustration as to why the assumption that all clumps of material in a circumstellar being spherical is not ideal. Provided these channels

are situated around 0.4AU from the star, the radius calculated would actually be length of the channel around the star that fell along the line of sight, and is not an indicator of the width of the channels.

4.5 Mass

The mass of material occulting a star was calculated assuming the material was spherical in shape and of a constant density. Figure 4.12 shows the distribution of mass values for all dips analysed. The majority of values fall below 1.5 lunar masses, aside from a small peak present between 2.7 and 3.7 lunar masses. As the dimensions were used as radii in calculations for mass and these values are dependent on the dip duration, this peak is most likely the result of the dips lasting upwards of 200 days. As there is uncertainty over the validity of the longest recorded dips, the mass distribution was cut to values less than 0.1 lunar masses (figure 4.13).

The distribution shown in figure 4.13 is similar in shape to the radius distribution in figure 4.11, containing values from the same dips. However, the distribution for mass narrower than the distribution for radii. For this to be the case, there must be a wide range in densities. The density distribution for all dips can be seen in figure 4.14, and shows that for most objects, the material density ranged from between 0.1kgm^{-3} up to 0.8kgm^{-3} with one small peak at 1.6kgm^{-3} , which is likely an outlier. These values represent the increase in density relative to the rest of the material in the disk. The consistently low density values provide explanation for the narrow range of mass values compared to radii values.

As the density distribution shows, most of the density values were very low, with some long dips giving higher values for the material size, this indicates large shifts in material which could be indicative of warps in the disks.

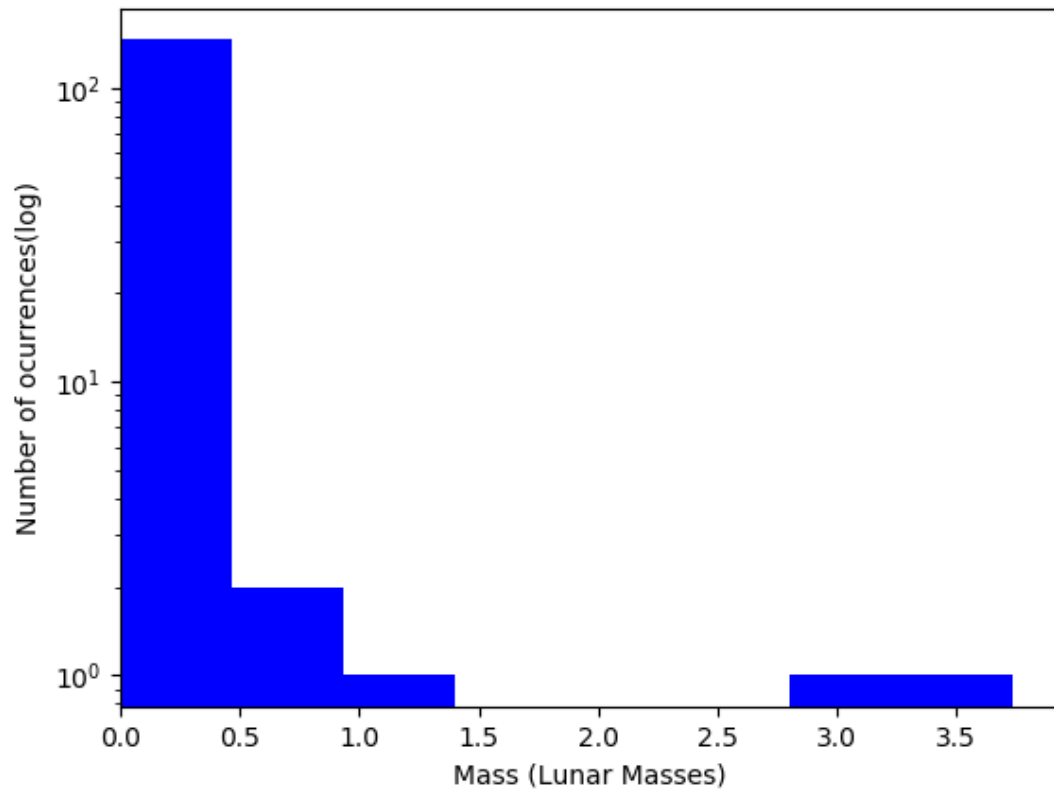


Figure 4.12: *histogram of distribution of the estimate mass of material occulting the star, calculated for every dip analysed, displayed in lunar masses*

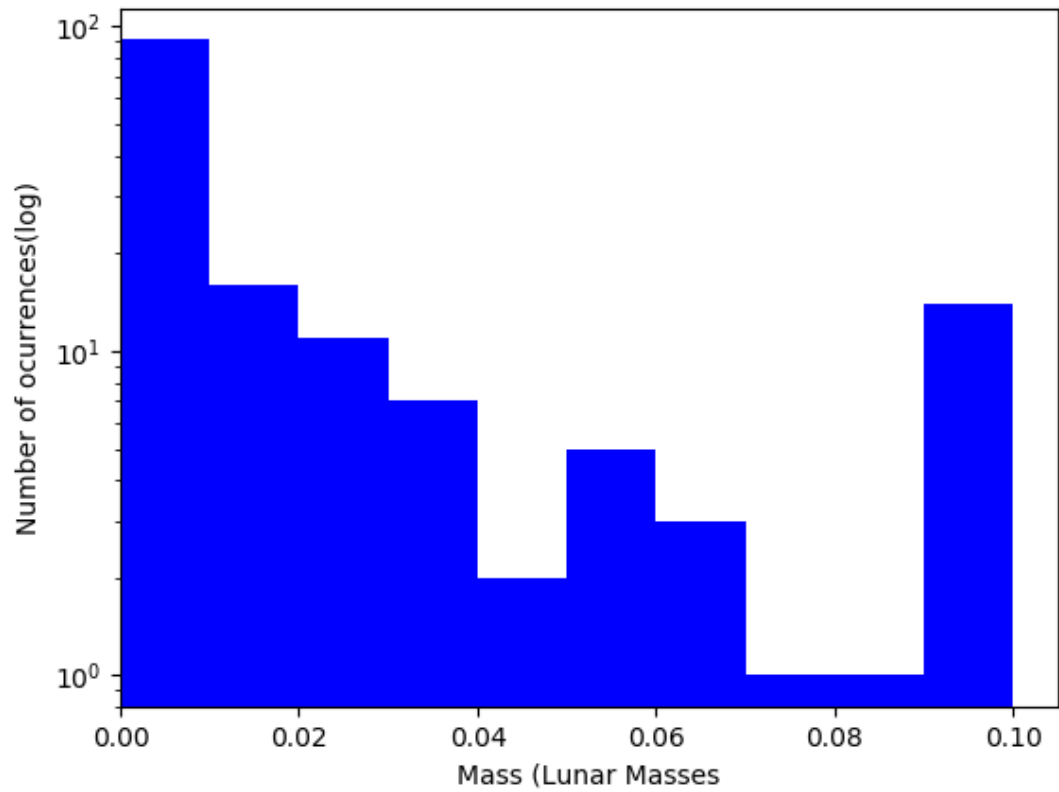


Figure 4.13: *Histogram of the distribution of mass values below 0.1 Lunar Masses*

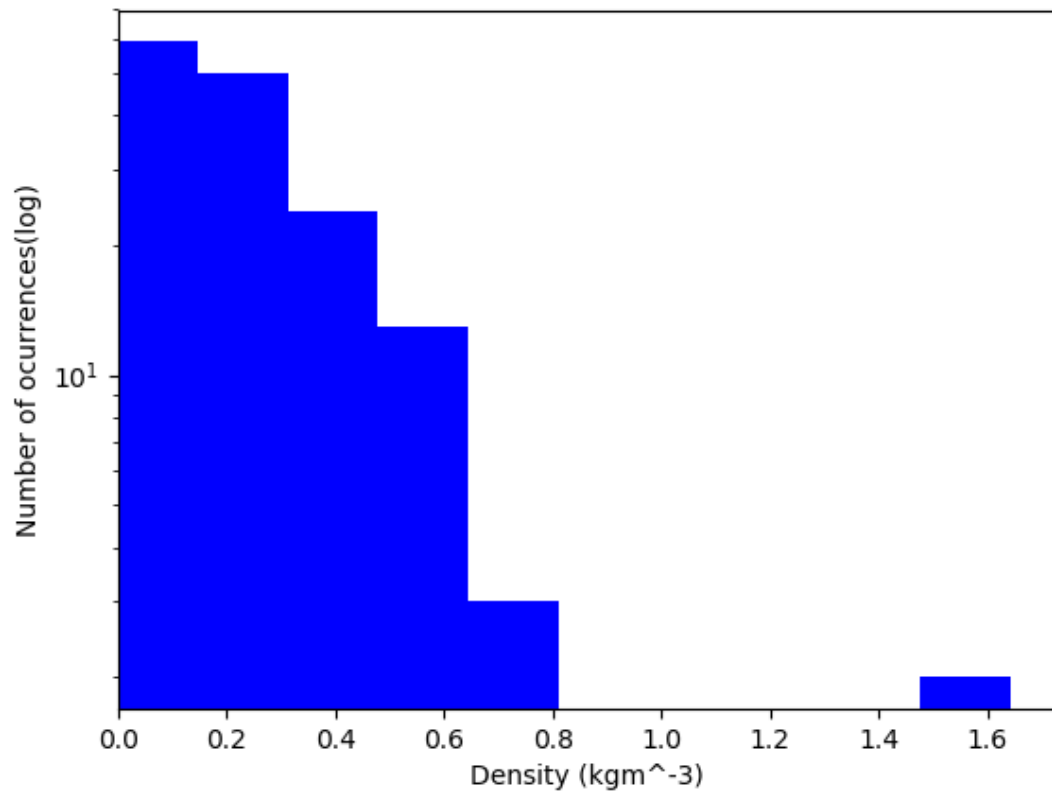


Figure 4.14: *Histogram of the density distribution across all dipoles analysed.*

4.6 Grain size

Across all of the objects observed, 263 were classified as having dips, including single data point dips. Of these, 163 objects contained only one dip, with that dip only containing one data point, meaning a gradient for the object's V against $V-I$ slope could not be found. Considering the expected number of dips due to noise, was 138 dips, dips due to noise may have potentially been removed. While there is no guarantee that the single data point dips removed were all noise, as there is only a 0.3% probability of noise being falsely classified as a dip, and rarely more than 200 data points per light-curve a false dip is statistically unlikely to occur multiple times in one light-curve. As discussed in section 4.1.1, there are far more dips containing single data points than the number of expected number of noise dips, meaning the vast majority of the single data point dips found are unlikely to be the result of noise. This left 100 objects where the V against $V-I$ gradient could be found. The distribution of these values is shown in figure 4.15, which shows apparent peaks at 45° , 65° , and 85° .

The peak at 65° was expected, as it indicates the presence of interstellar dust. This is the same as the gas and dust that make up a star's inner circumstellar disk. While it is not the largest peak on the graph, it shows that a reasonable number of the objects observed contain one or more dips, of any length, caused by material within the inner disk.

The peak seen at 85° can be explained by dense, optically thick material passing in front of the star. It is also characteristic of a multi-star system, although these are uncommon, and for this data sample, are not likely to be the cause for the peak.

The strongest peak in the distribution is at 45° and should be a subject for further investigation. This would normally be the result expected from noise, and may result from light-curves with multiple dips consisting of single data points. However, most of the single data point dips are caused by material from the circumstellar disk. As well as this, many single data point dips were removed from the distribution. In the occasion that a false dip was included when calculating the slope for a particular object, it is statistically very unlikely that the other dips in the light-curve were also invalid. As such, the overall

α value for the object would not be expected to be 45° , as the other dips present would effect the result. This could suggest that many of the legitimate dips recorded result in an α value similar to noise. It is possible that some objects were poorly filtered, which may have potentially lead to some dips not being defined properly, and this in turn could have affected the α values. Any object containing dips that give an α value of 45° should be investigated further to make sure the light-curve has been filtered effectively, however this was outside the scope of the project. If the light-curve has been filtered effectively, and the dips classified correctly, it could warrant an investigation into the cause of this behaviour.

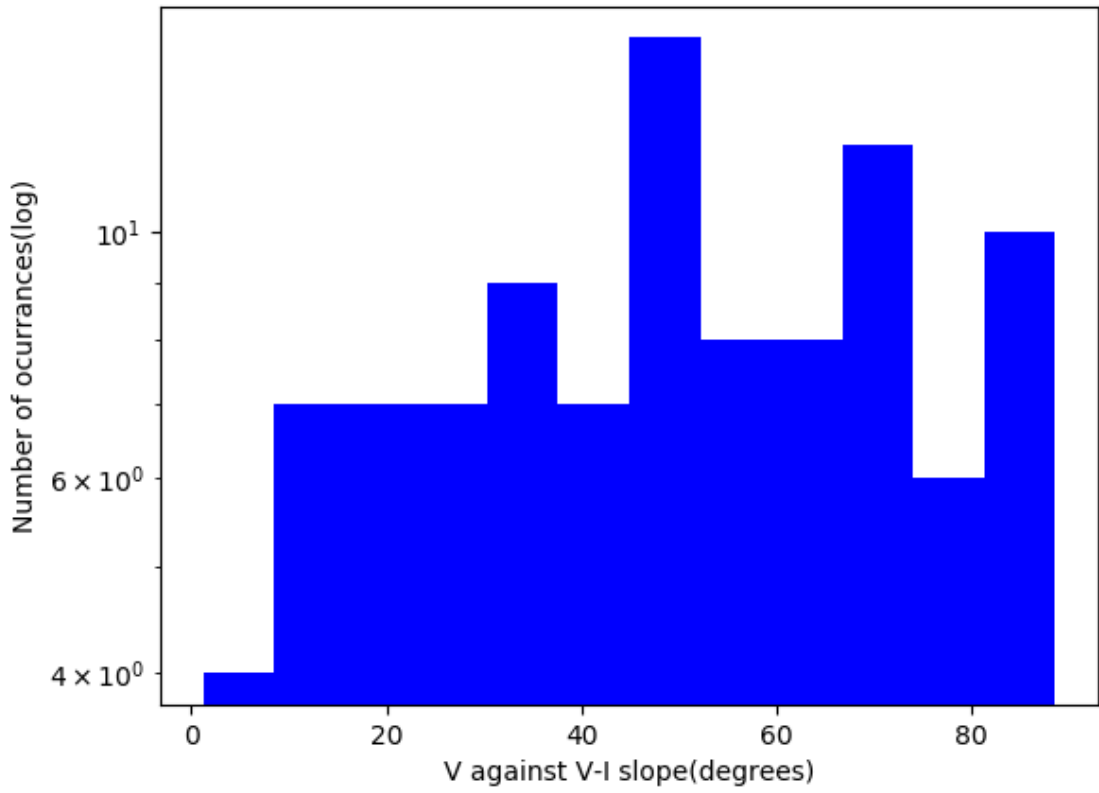


Figure 4.15: *Figure of the distribution of the values of the slopes of the V against V-I plots, in degrees.*

Chapter 5

Conclusions

In this thesis, the light-curves of nearby YSOs were analysed in the search for dipper stars. This was done with the intention of analysing their behaviour and build an understanding of the structure of the inner circumstellar disk. The depth and duration of the dips were measured and used to calculate the potential size and mass of material clumps causing the dips.

The distribution of dip depth and duration of dipper stars was consistent in comparison to previous work (Ansdell et al., 2016a, and Hedges, Hodgkin, and Kennedy, 2018). This proved that the dips defined were the result of inner disk material. However, there were some anomalous results, and observing those light-curves by eye showed that not all of the light-curves had been filtered properly. Future work could focus on ensuring that all light-curves are filtered correctly so that all dips present can be correctly defined.

The dimensions calculated for the material occulting the star were mostly low enough to be reasonable values for material in the inner disk. As some values of radius calculated were greater than the estimated distance of material from the star, more work will have to be put into working out the distance of material from the star. If this is done, an accurate value for radius can be calculated, and used to determine whether the material present is a near spherical clump, or a channel of material spiralling around the central

star. This would require an even longer set of data, and potentially patterns in the time difference between consecutive dips. Such information could lead to a detailed model of the structure of the inner circumstellar disks that surround dipper stars.

The distribution of mass was very narrow in comparison to the values for the dimensions of material, which was due to the very low density of the material. This further confirms that the dips recorded were due to fine gas and dust particles found in the inner disk.

When observing the α values, the expected peaks at 65° and 85° were observed and are explained respectively by interstellar dust and more optically thick material. However, the large peak at 45° is suspicious as it would normally be explained by noise. Considering the 0.3% chance of a data point being incorrectly being defined as a dip, and the number of objects removed due to insufficient data points in dips, the noise present should be minimal. Despite this, the peak at 45° was the strongest peak in the distribution, signifying another cause for this value. A future student can investigate the cause for this, be it an issue with filtering the light-curves, or otherwise.

Overall, the results of this thesis provides the starting blocks for creating a model of the inner circumstellar disks of young dipper stars. An effective method of defining dips in light-curves automatically has been made, with improvements to be made to using the ideal filter width for every object. The dimensions calculated for the material causing the dips has given insight into the possible types of structure that may be found in an accretion disk. Finally, the behaviour between the Visual and Infra-red filters has proven to be unusual, and could be an interesting topic for future investigation.

Bibliography

- Adams, F. C., C. J. Lada, and F. H. Shu (1987). “Spectral evolution of young stellar objects”. In: 312, pp. 788–806. DOI: 10.1086/164924.
- Andre, P., D. Ward-Thompson, and M. Barsony (2000). “From Prestellar Cores to Protostars: the Initial Conditions of Star Formation”. In: *Protostars and Planets IV*, p. 59. eprint: astro-ph/9903284.
- Ansdell, M. et al. (2016a). “Dipper discs not inclined towards edge-on orbits”. In: 462, pp. L101–L105. DOI: 10.1093/mnrasl/slw140. arXiv: 1607.03115 [astro-ph.EP].
- Ansdell, M. et al. (2016b). “Young “Dipper“ Stars in Upper Sco and Oph Observed by K2”. In: 816, 69, p. 69. DOI: 10.3847/0004-637X/816/2/69. arXiv: 1510.08853 [astro-ph.EP].
- Audard, M. et al. (2014). “Episodic Accretion in Young Stars”. In: *Protostars and Planets VI*, pp. 387–410. DOI: 10.2458/azu_uapress_9780816531240-ch017. arXiv: 1401.3368 [astro-ph.SR].
- Bae, Jaehan, Zhaohuan Zhu, and Lee Hartmann (2017). “On the Formation of Multiple Concentric Rings and Gaps in Protoplanetary Disks”. In: 850.2, 201, p. 201. DOI: 10.3847/1538-4357/aa9705. arXiv: 1706.03066 [astro-ph.EP].
- Bally, J. and N. Z. Scoville (1980). “Structure and evolution of molecular clouds near H II regions. I - CO observations of an expanding molecular shell surrounding the Pelican Nebula”. In: 239, pp. 121–136. DOI: 10.1086/158094.
- Bitsch, B. et al. (2015). “The structure of protoplanetary discs around evolving young stars”. In: 575, A28, A28. DOI: 10.1051/0004-6361/201424964. arXiv: 1411.3255 [astro-ph.EP].

- Bohlin, R. C., B. D. Savage, and J. F. Drake (1978). “A survey of interstellar H I from Lalpha absorption measurements. II.” In: 224, pp. 132–142. DOI: 10.1086/156357.
- Bouvier, J. et al. (1993). “Coyotes-I - the Photometric Variability and Rotational Evolution of T-Tauri Stars”. In: 272, p. 176.
- Bouvier, J. et al. (2003). “Eclipses by circumstellar material in the T Tauri star AA Tau. II. Evidence for non-stationary magnetospheric accretion”. In: 409, pp. 169–192. DOI: 10.1051/0004-6361:20030938. arXiv: astro-ph/0306551 [astro-ph].
- Chiang, E. I. and P. Goldreich (1999). “Spectral Energy Distributions of Passive T Tauri Disks: Inclination”. In: 519, pp. 279–284. DOI: 10.1086/307351. eprint: astro-ph/9812194.
- Cody, A. M. et al. (2014). “CSI 2264: Simultaneous Optical and Infrared Light Curves of Young Disk-bearing Stars in NGC 2264 with CoRoT and Spitzer_Evidence for Multiple Origins of Variability”. In: 147, 82, p. 82. DOI: 10.1088/0004-6256/147/4/82. arXiv: 1401.6582 [astro-ph.SR].
- Dahm, S. E. and T. Simon (2005). “The T Tauri Star Population of the Young Cluster NGC 2264”. In: 129, pp. 829–855. DOI: 10.1086/426326.
- Dunham, M. M. et al. (2014). “The Evolution of Protostars: Insights from Ten Years of Infrared Surveys with Spitzer and Herschel”. In: *Protostars and Planets VI*, pp. 195–218. DOI: 10.2458/azu_uapress_9780816531240-ch009. arXiv: 1401.1809.
- Elias, J. H. (1978). “A study of the IC 5146 dark cloud complex”. In: 223, pp. 859–861. DOI: 10.1086/156319.
- Engler, N. et al. (2019). “Investigating the presence of two belts in the HD 15115 system”. In: 622, A192, A192. DOI: 10.1051/0004-6361/201833542. arXiv: 1812.02750 [astro-ph.EP].
- Froebrich, D et al. (2018a). “A Survey for Variable Young Stars with Small Telescopes: First Results from HOYS-CAPS”. In:
- Froebrich, D. et al. (2018b). “Variability in IC5070: Two Young Stars with Deep Recurring Eclipses”. In: *Research Notes of the American Astronomical Society* 2.2, 61, p. 61. DOI: 10.3847/2515-5172/aacd48. arXiv: 1806.06608 [astro-ph.SR].
- Getman, K. V. et al. (2012). “The Elephant Trunk Nebula and the Trumpler 37 cluster: contribution of triggered star formation to the total population of an H II region”. In:

- 426, pp. 2917–2943. DOI: 10.1111/j.1365-2966.2012.21879.x. arXiv: 1208.1471 [astro-ph.SR].
- Gillen, E. et al. (2017). “CoRoT 223992193: Investigating the variability in a low-mass, pre-main sequence eclipsing binary with evidence of a circumbinary disk”. In: 599, A27, A27. DOI: 10.1051/0004-6361/201628483. arXiv: 1611.05461 [astro-ph.SR].
- Gruendl, R. A. and Y.-H. Chu (2009). “High- and Intermediate-Mass Young Stellar Objects in the Large Magellanic Cloud”. In: 184, pp. 172–197. DOI: 10.1088/0067-0049/184/1/172. arXiv: 0908.0347 [astro-ph.SR].
- Guarcello, M. G. et al. (2017). “CSI 2264: Simultaneous optical and X-ray variability in pre-main sequence stars. I. Time resolved X-ray spectral analysis during optical dips and accretion bursts in stars with disks”. In: 602, A10, A10. DOI: 10.1051/0004-6361/201629983. arXiv: 1701.04842 [astro-ph.SR].
- Guo, Zhen et al. (2018). “Star-Disk Interactions in Multiband Photometric Monitoring of the Classical T Tauri Star GI Tau”. In: 852.1, 56, p. 56. DOI: 10.3847/1538-4357/aa9e52. arXiv: 1711.08652 [astro-ph.SR].
- Haisch Jr., K. E., E. A. Lada, and C. J. Lada (2001). “Circumstellar Disks in the IC 348 Cluster”. In: 121, pp. 2065–2074. DOI: 10.1086/319951. eprint: astro-ph/0101486.
- Harvey, P. M. et al. (2008). “The Spitzer Survey of Interstellar Clouds in the Gould Belt. I. IC 5146 Observed With IRAC and MIPS”. In: 680, pp. 495–516. DOI: 10.1086/587687.
- Hedges, C., S. Hodgkin, and G. Kennedy (2018). “Discovery of new dipper stars with K2: a window into the inner disc region of T Tauri stars”. In: 476, pp. 2968–2998. DOI: 10.1093/mnras/sty328. arXiv: 1802.00409 [astro-ph.SR].
- Hensberge, H., K. Pavlovski, and W. Verschueren (2000). “The eclipsing binary V578 Mon in the Rosette nebula: age and distance to NGC 2244 using Fourier disentangled component spectra”. In: 358, pp. 553–571.
- Herbst, W. (2012). “The Variability of Young Stellar Objects”. In: *Journal of the American Association of Variable Star Observers (JAAVSO)* 40, p. 448.
- Ibryamov, S. et al. (2018). “Long-term BVRI photometric light curves of 15 PMS stars in the IC 5070 star-forming region”. In: *ArXiv e-prints*. arXiv: 1805.11745 [astro-ph.SR].
- Johns-Krull, C. M., J. A. Valenti, and C. Koresko (1999). “Measuring the Magnetic Field on the Classical T Tauri Star BP Tauri”. In: 516, pp. 900–915. DOI: 10.1086/307128.

- Johnstone, C. P. et al. (2014). “Classical T Tauri stars: magnetic fields, coronae and star-disc interactions”. In: 437, pp. 3202–3220. DOI: 10.1093/mnras/stt2107. arXiv: 1310.8194 [astro-ph.SR].
- Joy, A. H. (1945). “T Tauri Variable Stars.” In: 102, p. 168. DOI: 10.1086/144749.
- Lada, C. J. et al. (1994). “Dust extinction and molecular gas in the dark cloud IC 5146”. In: 429, pp. 694–709. DOI: 10.1086/174354.
- Lada, E. A. and C. J. Lada (1995). “Near-infrared images of IC 348 and the luminosity functions of young embedded star clusters”. In: 109, pp. 1682–1696. DOI: 10.1086/117396.
- Luhman, K. L. et al. (2003). “A Census of the Young Cluster IC 348”. In: 593, pp. 1093–1115. DOI: 10.1086/376594. eprint: astro-ph/0304409.
- Matthews, H. I. (1979). “High resolution radio observations of bright rims in IC 1396”. In: 75, pp. 345–350.
- McCabe, C.-E. (2004). “On the road to planets: T Tauri disk evolution”. PhD thesis. University of California, s Angeles, California, USA.
- Megeath, S. T. et al. (2004). “Initial Results from the Spitzer Young Stellar Cluster Survey”. In: 154, pp. 367–373. DOI: 10.1086/422823. eprint: astro-ph/0406008.
- Meng, H. Y. A. et al. (2017). “The First 40 Million Years of Circumstellar Disk Evolution: The Signature of Terrestrial Planet Formation”. In: 836, 34, p. 34. DOI: 10.3847/1538-4357/836/1/34. arXiv: 1701.01786 [astro-ph.SR].
- M.Fernandez, C. Eiroa (1996). “Variability of Classical T Tauri Stars”. In: *Astronomy and Astrophysics*.
- Park, B.-G. and H. Sung (2002). “UBVI and H α Photometry of the Young Open Cluster NGC 2244”. In: 123, pp. 892–904. DOI: 10.1086/338643.
- Perez, M. R., P. S. The, and B. E. Westerlund (1987). “On the distances to the young open clusters NGC 2244 and NGC 2264”. In: 99, pp. 1050–1066. DOI: 10.1086/132077.
- Reach, W. T. et al. (2004). “Protostars in the Elephant Trunk Nebula”. In: 154, pp. 385–390. DOI: 10.1086/422193. eprint: astro-ph/0406308.
- Schmeja, S., R. S. Klessen, and D. Froebrich (2005). “Number ratios of young stellar objects in embedded clusters”. In: 437, pp. 911–918. DOI: 10.1051/0004-6361:20041898. eprint: astro-ph/0503611.

- Stelzer, B. and A. Scholz (2009). “A Chandra and Spitzer census of the young star cluster in the reflection nebula NGC 7129”. In: 507, pp. 227–240. DOI: 10.1051/0004-6361/200912315. arXiv: 0907.4252 [astro-ph.SR].
- Straižys, V. et al. (2014). “The distance to the young cluster NGC 7129 and its age”. In: 438, pp. 1848–1855. DOI: 10.1093/mnras/stt2334. arXiv: 1312.1153.
- Strom, S. E., G. L. Grasdalen, and K. M. Strom (1974). “Infrared and optical observations of Herbig-Haro objects.” In: 191, pp. 111–142. DOI: 10.1086/152948.
- Ungerechts, H. and P. Thaddeus (1987). “A CO survey of the dark nebulae in Perseus, Taurus, and Auriga”. In: 63, pp. 645–660. DOI: 10.1086/191176.
- Williams, J. P. and L. A. Cieza (2011). “Protoplanetary Disks and Their Evolution”. In: 49, pp. 67–117. DOI: 10.1146/annurev-astro-081710-102548. arXiv: 1103.0556 [astro-ph.GA].
- Yorke, H. W. and E. Kruegel (1977). “The dynamical evolution of massive protostellar clouds”. In: 54, pp. 183–194.